8-2016

Particle Separation Using Electrokinetically-Driven Deterministic Lateral Displacement: A Computational Study

Xuchen Liu
Clemson University, xuchenl@g.clemson.edu

PARTICLE SEPARATION USING ELECTROKINETICALLY-DRIVEN DETERMINISTIC LATERAL DISPLACEMENT: A COMPUTATIONAL STUDY

A Thesis

Presented to

the Graduate School of

Clemson University

In Partial Fulfillment

of the Requirements for the Degree

Master of Science

Mechanical Engineering

---

by

Xuchen Liu

August 2016

Accepted by:

Dr. Xiangchun Xuan, Committee Chair

Dr. Lonny Thompson

Dr. Rodrigo Martinez-Duarte

ABSTRACT

Electrokinetically-driven deterministic lateral displacement (e-DLD) is a recently proposed technique for continuous, two-dimensional fractionation of particle suspensions in microfluidic platforms. It utilizes the negative dielectrophoretic force that is induced by the DC electric field gradients formed around an array of regularly spaced posts. While e-DLD devices have been demonstrated to be able to separate particles by size, a fundamental understanding of the separation process and the factors that affect the separation is still lacking. This thesis is aimed to answer these questions using a computational study of electrokinetic particle transport and separation in e-DLD devices.

We first numerically prove a continuous, two-dimensional separation of 5 μm, 10 μm and 15 μm-diameter rigid circular particles in an e-DLD device. These particles can be viewed as good mimics of red blood cells, white blood cells and tumor cells, respectively, in blood. A number of features are observed in the kinetics of particles, including directional locking and sharp transitions between migration angles upon variations in the direction of the force, which are advantageous for high-resolution two-dimensional separation.

We then discuss several factors that affect the separation of particles in the proposed e-DLD device, such as electric field, forcing angle, post gap ratio, post shape and particle shape. We find that the electric field influences the particle separation by affecting the electric field gradient. The larger electric field, the larger electric field gradient will be. We also investigate the orientation of the driving field with respect to the array of posts and find that, at specific forcing-angles, particles of different sizes migrate in different directions, enabling continuous, two-dimensional separation in electrokinetic flow.

Moreover, we study the effect of the post gap ratio on particle separation. The smaller the ratio, the larger the electric field gradient will be around the posts, so particles will more easily get deflected away from the posts due to the enhanced negative dielectrophoretic force.

In addition, we find that the shape of posts plays an important role in particle separation. Using equilateral triangular posts, we are able to separate smaller particles as compared to the traditional circular posts under the same conditions. We also look into the effect of particle shape on separation in e-DLD. It is found that an elliptic particle behaves like a smaller sized circular particle due to its preferred orientation in electric field. Therefore, we can easily achieve the separation of circular and elliptic particles with an equal surface area.

In the end, we compare e-DLD with the traditional pressure-driven DLD. With the same geometry, e-DLD device is capable of separating much smaller particles. Alternatively, pressure-driven DLD requires a smaller gap size and/or a smaller forcing angle to implement the same particle separation which will make the manufacture harder. Using e-DLD device will considerably ease the DLD device fabrication and shorten the length of the post array.

DEDICATION

I dedicate this dissertation to my grandfather, who would have felt proud to see me earn a Master. I also dedicate my research to my undergraduate institute, Beijing Institute of Technology (BIT), which let me take my first step into the Mechanical Engineering world.

ACKNOWLEDGMENTS

First of all, I would like to thank my advisor, Dr. Xiangchun Xuan, for providing me the opportunity to work in this field for the past two years. Specifically, I would like to express my strong and sincere gratitude to him for his broad foresight, patient and positive guidance, thorough tutoring, and unwavering support on my research which not only enhanced my career growth but also paved the way for my academic career.

Then, I would also like to thank my committee members, Dr. Lonny Thompson, Dr. Rodrigo Martinez-Duarte for taking precious time from their busy schedule and offering me extensive and constructive suggestions and guidance on my research. Their suggestions have helped a lot in improving the quality of my work.

I would express my sincere gratitude to the mechanical engineering department for providing me a consistent financial support through graduate assistantships. I also thank the entire support team of the Palmetto Cluster for consistently providing their valuable support for resolving the simulation issues. This research would not have been possible without them.

My colleagues have always been a source of inspiration for me, and have consistently provided me valuable inputs on my research as well as teaching methods in some way or the other. I would like to especially thank Xinyu for his patient help, without his help, I could never make this far. I would also like to sincerely thank my lab mates, Asher, Di, Rama and Yilong for being a wonderful support during my graduate research.

Last but certainly the most important, I am indebted to girlfriend Hangjin and my parents for being the pillars of my life. I have always felt overjoyed and refreshed after meeting or speaking to them, and this has significantly helped me look at life optimistically and overcome my professional frustrations. Without their unconditional love, support, blessings and motivation, I would never have managed to be what I am today.

TABLE OF CONTENTS

Page

Table of Contents (Continued)

Page

LIST OF TABLES

Page

LIST OF FIGURES

Page

List of Figures (Continued)

Page

List of Figures (Continued)

Page

List of Figures (Continued)

Page

List of Figures (Continued)

Page

CHAPTER ONE

INTRODUCTION

1.1 Motivation

Over the last decades, microfluidics-based lab-on-a-chip (LOC) devices have promised to offer numerous advantages over conventional analysis techniques by manipulating fluids and samples in channels with dimensions of tens of micrometers. The advantages include small quantities of samples and reagents, high resolution and sensitivity, low cost, short time for analysis, small footprints for the analytical devices[1].

Particle manipulation is very essential in lab-on-a-chip device since it has broad applications in industry. Generally, particle manipulation includes pumping, focusing, trapping, concentration, separation, and sorting. As an overview, particle separation is one of the most fundamental manipulation functions in microfluidic devices, and refers to transforming a mixture of particles into two or more distinct sub-streams. In medical and biological fields, particle separation is an essential sample processing step, allowing researchers to do the work on micro-particles, bacteria, cells and viruses. Existing microfluidic separation methods can be categorized as either active or passive, where active methods incorporate an external force and passive methods rely on carefully designed channel geometries and internal forces to separate particles in different properties[2]. Some common active separation methods include dielectrophoresis, electrophoresis, acoustophoresis, immunomagnetic separation (IMS), flow cytometry or FACS and optical force[3-5].Alternatively, some passive methods adopted to differentiate

between particles are the use of pillars, weirs and objects within micro-channels, adhesion-based methods, pinched-flow fractionation (PFF)[6, 7], hydrodynamic filtration (HDF)[8], hydrophoretic separation[9], Brownian ratchet separation[10], asymmetric cavity flow[11], inertial forces and biomimetic separation[3,12].

Among the methods of particle separation, separation using electrokinetics, which transports particles by the application of electric fields, has received much attention for its simplicity and effectiveness in performing these operations: electrokinetic flow is easy to control and integrate with a plug-like flow. Many studies of particle separation using electrokinetic flow have been published[13-15]. In this thesis, we will focus on a promising separation methods which also uses electrokinetics— e-DLD.

DLD device is one of the most efficient separation methods which are widely used now. Some of the external forces have been used in DLD, including acoustic[16], electric[17,18], gravitational[19,20,21]. Dielectrophoretic (DEP) force is one of the most widely used non-linear electrokinetic mechanism to manipulate particles. It is caused by polarization effects when a dielectric particle, cell or virus is exposed to a non-uniform electric field.

As we mentioned before, particle separation methods can be categorized as active, passive and hybrid methods, in some cases, hybrid microfluidic separation devices that combine passive and active separation techniques enhance the separation performance, e-DLD is one of them. To date, a lot of works on pressure-driven DLD separation have been published[22-25], however, studies on e-DLD devices are not complete. Drazer first demonstrated experimentally different sizes of suspended particles migrated in different trajectories at certain geometries in microfluidic devices using electrokinetically-driven

deterministic lateral displacement (e-DLD)[26]. However, very few numerical studies have been done to prove e-DLD devices' capability, and not many factors have been studied in e-DLD devices. In this thesis, we first use numerical simulations to prove the e-DLD devices' ability to separate particles by size. And then we discuss the factors that affect the particle separation in e-DLD devices. In the end, we compare the e-DLD devises with pressure-driven DLD devices and show the advantages of e-DLD devices. The goal is to obtain a fundamental knowledge of electrokinetic particle transportation in e-DLD devices.

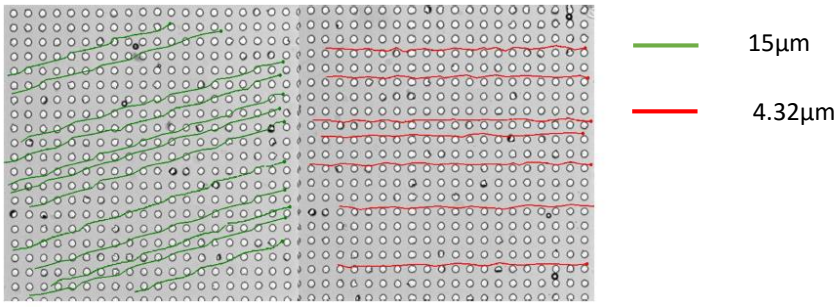

Fig. 1 Different sizes of particles migrate in different trajectories at certain geometries in experiment using e-DLD device by Huang et al.

1.2 Background on Electrokinetic Phenomena

The first observation of electrokinetic phenomena dates back to the studies conducted by Reuss in 1809, however, the first theoretical developments of electrokinetic transport are attributed to Helmholtz and Smoluchowski[27, 28]. The follow-up development of these early works has been summarized by Dukhin and Derjaguin[29]. Since then, considerable attention has been conferred on electrokinetic phenomena.

Electrokinetics refers to the use of the electric field to exert electrostatic forces on charged or polarizable fluids and suspended particles, which in turn induces the motions

of fluids and particles. With significant advancement in micro-/nano fabrication technology, electric field can be scaled down to the micro-/nanoscale, in which electrokinetics becomes one of the most promising techniques to transport and manipulate particles. The general classification of electrokinetic-phenomena is the following: 1. Electric double layer which refers to a region close to a solid-liquid interface which experiences a non-zero net charge density of ions. 2. Electroosmosis which refers to the movement of an ionized fluid under the effect of an electric field. 3. Electrophoresis which refers to the movement of charged particles by an electric field in a resting fluid. 4. Dielectrophoresis which refers to the movement of dielectric particles by the existence of an electric field gradient. This thesis will focus on electrokinetic phenomena using an applied electric field to induce motion and hence accompanying background on electrokinetic transport, electro-osmosis, electrophoresis, and dielectrophoresis will be discussed in depth as follows.

1.2.1 The Electric Double Layer

In general, most solid surfaces tend to gain surface charges when they are brought into contact with ionic aqueous solutions. When this surface comes in contact with an electrolyte solution, it attracts the ions of opposite charge called counter-ions towards it and repels those of like charge called co-ions away from it. The electrostatic interaction between the charged surface and the surrounding ions attracts counter-ions and repels co-ions from the charged surface. As a results, a thin layer predominantly occupied with more counter-ions is formed in the vicinity of the charged surface, referred to as the EDL. Usually all the solid surfaces acquire charges due to various mechanisms such as

ionization of surface groups, isomorphic substitutions of charged groups, charged crystal surfaces and specific adsorption of ions. Hence, initially the concentration of the counter-ions close to the channel wall is very high. This high concentration induces a diffusive effect back into the bulk fluid away from the wall. As a consequence of these opposing effects of electrostatic attraction and diffusive repulsion, an equilibrium distribution of counter-ions is created normal to the solid surface. The concentration, and hence the charge density of counter-ions is higher than that of the co-ions close to the solid surface. The concentrations of both types of ions become equal in the bulk, to maintain electroneutrality. At the same time, the presence of unbalanced charges of the counter-ions generates an equilibrium distribution of an electric potential. It follows a trend identical to the concentration distribution, ranging from a high potential close to the surface to vanish in the bulk fluid. The distributions of the potential and concentration of counter-ions and is illustrated in Figure 2.

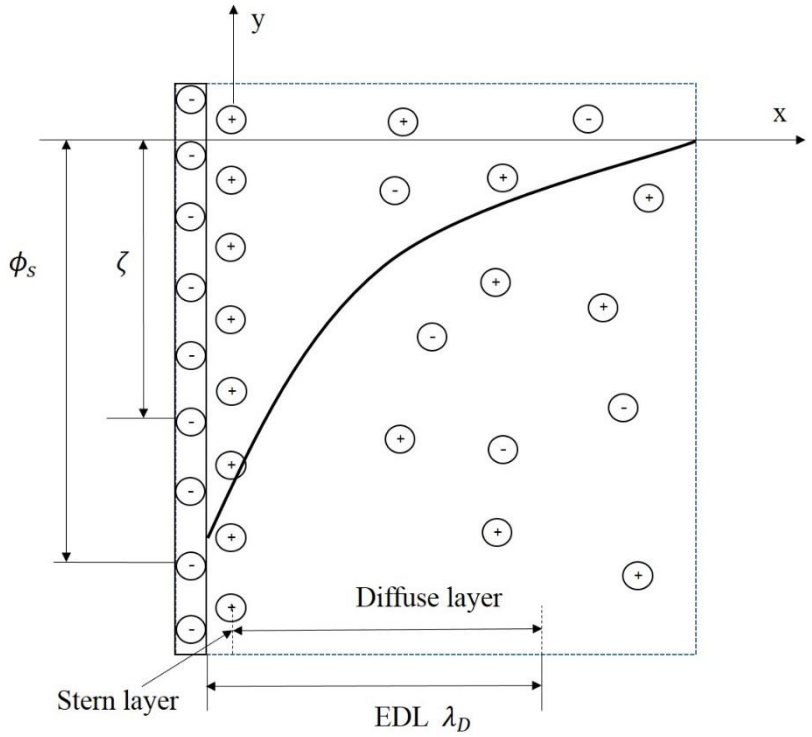

Fig. 2 Schematics of an EDL formed adjacent to a negatively charged planar surface

Very close to the solid surface (See Fig 1), lies a thin layer of the counter-ions tightly bound to the solid surface. This is called the Stern Layer and its thickness is typically of the order of one or two times the diameter of the counter-ions. The electric potential is assumed to drop linearly across the Stern Layer[30]. Outside the Stern Layer, lies a region which experiences the motion of ions into and out of the same due to the opposing effects of electrostatic attraction and diffusive repulsion, although the equilibrium concentration distribution is maintained. This region is called the Diffuse Layer, and it is separated from the Stern Layer by an imaginary interface called the Slip Plane. Ions within the stern layer are immobilized due to a very strong electrostatic force; ions within the diffuse layer are free to move. As a result, we mainly focus on the diffuse layer. The Gauss' law of charge

conservation can be used to relate the electric potential in the diffuse layer to the local charge density as,

$$\nabla \cdot (\varepsilon \nabla \varphi) + \rho_E = 0 \qquad (1)$$

Equation 1.1 dictates the existence of a non-zero charge density ρ_E in presence of an electric potential distribution φ, and hence an electrolyte solution in contact with a solid wall experiences a net charge density of the counter-ions. The electric potential in the diffuse layer has been obtained by analytically solving equation 1.1 and has been demonstrated to follow either an exponential or a hyperbolic tangent decay to vanish in the bulk fluid, depending on the situations.

In summary, the EDL is a small volume of fluid close to the solid surface, composed of the immobile Stern Layer and the Diffuse Layer. Within the EDL the net electric potential in the fluid is non-zero due to the formation of the Boltzmann distribution of counter-ions. The thickness of the electric double layer is characterized by a parameter called the Debye length λ_D, which is expressed mathematically as,

$$\lambda_D = \sqrt{\frac{\varepsilon k_B T}{2z^2 e^2 C_0 N_A}} \qquad (2)$$

where ε, C_0 are respectively the fluid electric permittivity and the bulk counter-ion concentration at an absolute temperature T. N_A and k_B are the Avogadro's constant (6.023×10^{23} / mole) and the Boltzmann constant (1.38×10^{-23} J / K) respectively. The valence of the counter-ions species is given by "z" and "e" is the fundamental charge of 1.602×10^{-19} C. The Debye length usually ranges in the order of a few nanometers to a few hundred nanometers. Since the Stern Layer has an extremely small thickness and

does not contribute to the motion of ions in any manner, its presence in the fluid is commonly neglected. Hence the full analysis of the EDL is approximated very well using the Diffuse Layer alone, by assuming the Slip Plane, and hence the Zeta Potential on the solid surface.

1.2.2 Electroosmosis

When an external electric field is applied to a stationary charged surface, the excessive counter-ions within the EDL of the charged surface migrate toward the oppositely charged electrode, dragging the viscous fluid with them[31]. The induced flow motion arising from the electrostatic interaction between the net charge within the EDL and the applied electric field is called electroosmosis, also called electroosmotic flow (EOF), as shown in Figure 2.

According to Equation (3) (Coulombs law), Equation (4) (Navier-Stokes equation) and Equation (5) (Continuity equation):

The electrokinetic force acting on the liquid is written as

$$\mathbf{F} = \mathbf{E}\sum_{i=1}^{n} Fz_i c_i = -\varepsilon_0 \varepsilon_f \nabla^2 \phi \mathbf{E} \tag{3}$$

Where **E** is the externally applied electric field. Therefore, the fluid motion is governed by the modified Navier-Stokes (NS) equation,

$$\rho\left(\frac{\partial \mathbf{u}}{\partial t} + \boldsymbol{u}\cdot\nabla\boldsymbol{u}\right) = -\nabla p + \mu\nabla^2\mathbf{u} - \varepsilon_0\varepsilon_f\nabla^2\phi\mathbf{E} \tag{4}$$

and the continuity equation

$$\nabla\cdot\mathbf{u} = \mathbf{0} \tag{5}$$

Where ρ is the fluid density; **u** is the fluid velocity; p is the pressure; and μ is the fluid dynamic viscosity.

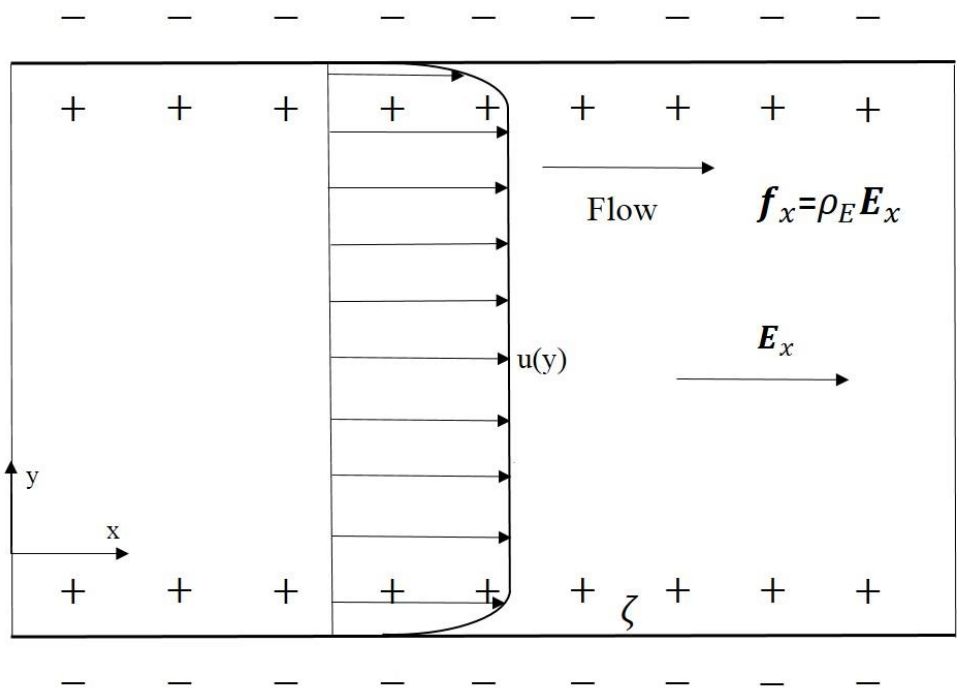

Fig. 3 Schematics of EOF in a slit channel bearing a uniform negative surface charge

Using above equations and applied no slip boundary condition, as the electric potential due to the surface charge decays to zero in the bulk region, the velocity in the bulk region remains a constant:

$$\mathbf{u}_{\mathrm{EO}} = -\frac{\varepsilon_0 \varepsilon_f E_x \zeta_w}{\mu} \tag{6}$$

where ζ_w is the zeta potential of the channel wall. With the thin EDL approximation, the EOF velocity profile in a microchannel is about uniform, referring to a plug like flow. Therefore, one can use the constant velocity to describe the EOF velocity outside the

EDL, which is known as the famous Smoluckowski slip velocity. Define $-\frac{\varepsilon_0\varepsilon_f\zeta_w}{\mu}$ as the electroosmotic mobility.

1.2.3 Electrophoresis

Electrophoresis refers to the migration of charged particles suspended in an aqueous solution subjected to an external electric field, as shown in Figure 3. The charges surface is stationary in EOF; however, it becomes mobile in electrophoresis.

The particle's electrophoretic velocity can be written as

$$\mathbf{U}_\mathrm{p} = \eta\mathbf{E} \tag{7}$$

Where η is the particle's electrophoretic mobility, under a thin EDL, the mobility of a particle suspended in an unbounded medium is described as $\frac{\varepsilon_0\varepsilon_f\zeta_\mathrm{p}}{\mu}$, where ζ_p is the zeta potential of the particle. The electrophoretic velocity is:

$$\mathbf{U}_\mathrm{EP} = \frac{\varepsilon_0\varepsilon_f\zeta_\mathrm{p}E_x}{\mu} \tag{8}$$

Let ε_m ($\varepsilon_\mathrm{m} = \varepsilon_0\varepsilon_\mathrm{f}$) be the absolute permittivity of the suspending medium, define electrokinetic mobility, $\mu_{EK} = \varepsilon_m(\zeta_p - \zeta_w)/\mu$ is estimated from the particle's electrokinetic velocity (sum of fluid and electrophoresis velocity) under small DC voltage in a straight channel. The electrokinetic velocity is defined as:

$$\mathbf{U}_\mathrm{EK} = \frac{\varepsilon_m(\zeta_\mathrm{p}-\zeta_\mathrm{w})\mathrm{E_x}}{\mu} \tag{9}$$

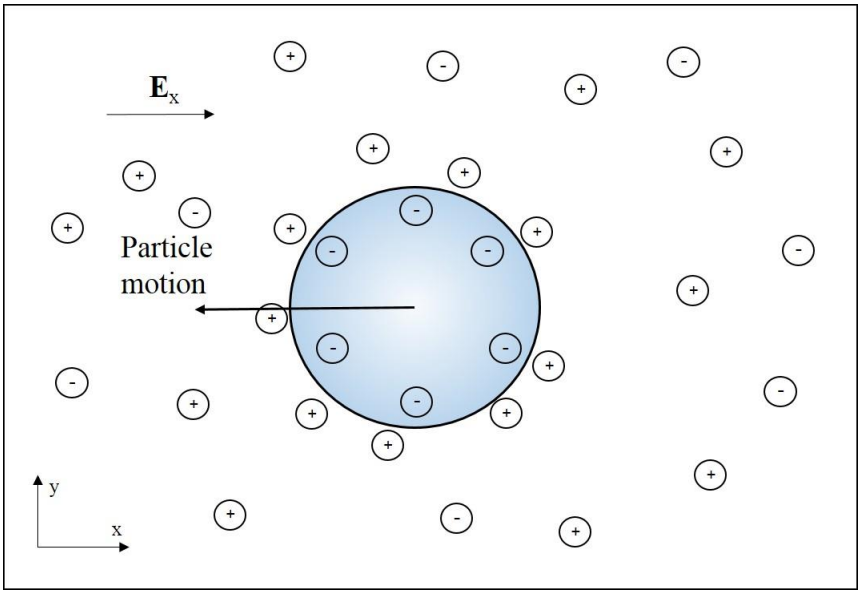

Fig. 4 Schematics of electrophoretic motion of a negatively charged particle under an imposed electric field

1.2.4 Dielectrophoresis

Dielectrophoresis refers to the motion of polarizable particles immersed in an aqueous solution subjected to a spatially non-uniform electric field. The ratio of the polarizability of particles to that of the electrolyte solution determines the direction of the DEP force. A positive (negative) dielectrophoresis refers to the DEP force directed toward (away from) the region with a higher electric field. The DEP force is proportional to the square of the electric field, indicating nonlinear electrokinetics. In addition, the DEP force is proportional to the third power of the particle size. The DEP force acting on a particle depends on the relative properties of the particle and the suspending medium; particles with a higher polarizability than that of the suspending medium exhibit positive DEP, and move towards the regions with higher electric field gradient. Negative DEP occurs when particles are repulsed from these regions. The behavior is expressed by the Clausius-

Mossoti (CM) factor: f_{CM} . When the particle is more polarizable than the fluid (i.e. $\sigma_p > \sigma_m$), f_{CM} is positive, a positive DEP force is generated and the particle moves from the low electric field region to the high electric field region. This is termed as positive DEP or p-DEP (Figure 4a). On the contrary if the particle is less polarizable than the fluid (i.e. $\sigma_p < \sigma_m$), f_{CM} becomes negative and the particles move from the high electric field region to the low electric field region. This is termed as negative DEP or n-DEP (Figure 4b). For DC dielectrophoresis, as the frequency of the applied electric field is zero, the f_{CM} can be expressed as:

$$f_{\mathrm{CM}} = \frac{\sigma_p - \sigma_m}{\sigma_m} \tag{10}$$

Using this feature, we can use DEP to manipulate particles and cells.

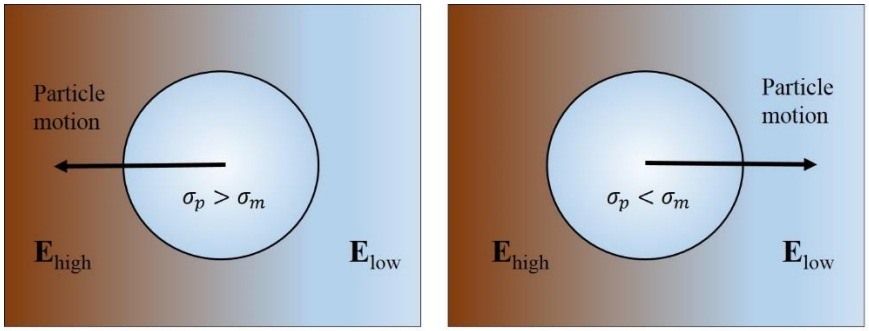

Fig 5. Schematics representations of dielectrophoresis of a spherical particle in a non-uniform electric field. (a) The particle moves with a positive DEP from low electric field to high electric field when more polarizable than the fluid. (b) The particle moves with a negative DEP from high electric field to low electric field when less polarizable than the fluid.

The DC DEP force acting on a spherical particle of radius r obtained by a point diploe method is expressed as:

$$\mathbf{F}_{\mathrm{DEP}} = 2\pi r^3 \varepsilon_0 \varepsilon_f f_{\mathrm{CM}} \nabla |\mathrm{E}_{\mathrm{rms}}|^2 \quad (11)$$

Where $\mathrm{E}_{\mathrm{rms}}$ is the root mean square electric field strength. The applied electric field $\mathbf{E} = -\nabla\phi$ is related to the electric potential.

The drag force on a spherical particle is

$$\mathbf{F}_{\mathrm{drag}} = 6\pi\mu r(\mathbf{u} - \mathbf{u}_{\mathrm{p}}) \quad (12)$$

At the creeping flow limit, which is known as Stokes law, where r is the particle radius, $\mathbf{u}$ is the fluid velocity, $\mathbf{u}_{\mathrm{p}}$ is the particle velocity. For the particle size considered in this study, the characteristic time scale of acceleration period of motion is much smaller than the time scale of the variation of the fluid variables. Therefore, the acceleration process can be neglected and it can be assumed that the particles move with the terminal speed all the time, which means the DEP force and drag force acting on the particle is equal and has opposite direction[32]. Equal equation (8) and (9), we can get the DEP velocity of the particle:

$$\mathbf{u}_{\mathrm{DEP}} = \frac{\varepsilon_{\mathrm{m}} r^2 f_{\mathrm{CM}}}{3\mu} \nabla \mathrm{E}_{\mathrm{rms}}^2 \quad (13)$$

Where ε_{m} ($\varepsilon_{\mathrm{m}} = \varepsilon_0 \varepsilon_{\mathrm{f}}$) is the absolute permittivity of the suspending medium.

The net speed of particle $\mathbf{U}_{\mathrm{p}}$ is:

$$\mathbf{U}_{\mathrm{p}} = \mathbf{U}_{\mathrm{EO+}}\mathbf{U}_{\mathrm{EP}} + \mathbf{U}_{\mathrm{DEP}} = \mathbf{U}_{\mathrm{EK}} + \mathbf{U}_{\mathrm{DEP}} \quad (14)$$

Dielectrophoresis is also classified according to the mechanism by which the electric field gradients are created in the microfluidic devices. The commonly used mechanisms are e-DEP and i-DEP.

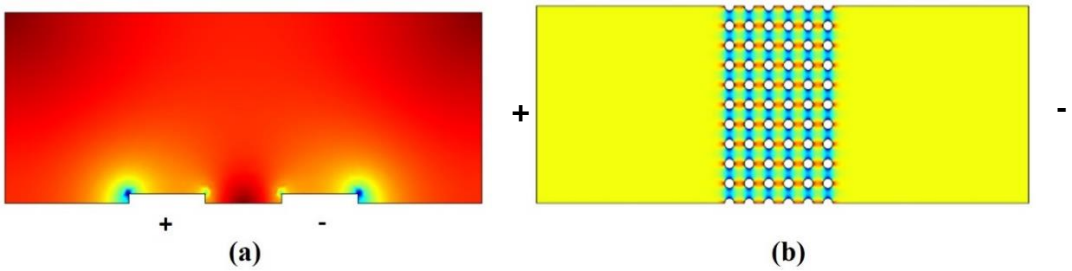

Fig 6. Schematics of the commonly used mechanisms for generation of electric field gradients (a) e-DEP (b) i-DEP. The "+" and "-" signs represent a voltage drop across a microchannel which generates an electric field. The electric field ranges from a high field intensity (blue) to low field intensity (red), thereby indicating the generation of gradients.

In electrode-based dielectrophoresis or e-DEP, the gradients are created by fabricating microelectrodes in the microchannel and applying a voltage. The fluid is pumped usually by pressure drop as DC electric field can cause a quick degradation of the in-channel microelectrodes. The method of e-DEP, similar to electrophoresis, has been studied and substantially used for manipulation of particles[33-35]. Although e-DEP offers strong local electric field gradients by applying small voltages, the concerned micro-devices are sometimes complicated to fabricate due to the need for introducing microelectrodes.
In addition, the e-DEP devices also suffer from a limitation of the potential electrode fouling in the zone of particle manipulation due to chemical reactions.
Electrodeless dielectrophoresis is a mechanism of generating electric field gradients by fabricating a microchannel geometry having non-uniform cross sections (Insulator-based Dielectrophoresis or i-DEP). At the most situations, the electrodeless DEP micro-channels are much simpler and cheaper to fabricate than e-DEP micro-channels since their design does not necessitate the fabrication of microelectrodes. Instead the electric field is applied across macroscopic metal electrodes that are introduced in far-field fluid reservoirs at the ends of the microchannel. The absence of microelectrodes also

minimizes the possibility of the fouling of electrodes in the zone of interest. In addition, the electric field responsible for generating gradients in these devices can also be used to pump the fluid electroosmotically at low flow rate. In the case of i-DEP, the charge conservation and the confinement of electric field within the microchannel generates a higher electric field at smaller cross sections, and a lower electric field at the larger cross sections. The resulting gradients in electric field are then used to manipulate particles / species. In i-DEP systems, electrophoresis (EP) and electroosmotic (EO) flow effects are significant, since usually high direct current (DC) or low frequency alternate current (AC) potentials are employed. Both phenomena (EP and EO) are linear functions of the electric field, giving rise to electrokinetics (EK), defined as the superposition of EO flow and EP. The use of i-DEP micro-devices to focus, trap, concentrate and separate species has been extensively demonstrated[36-41].

In summary, in e-DEP systems, arrays of microelectrodes are used to create non-uniform electric fields. The i-DEP system is actually the combination of both active and passive separation method. For active part, electroosmotic force, electrophoretic force and DEP force will act on the particle; for passive part, the insulating post will be used to generate non-uniform electric field. In i-DEP devices, the non-uniformities of the electric field are caused by the presence of insulating structures that distort the electric field distribution.

1.3 DLD device

1.3.1 Mechanism of DLD device

Deterministic lateral displacement (DLD) is a fractionation technique that can be implemented in all active, passive and hybrid modes. Deterministic lateral displacement is a technology which utilizes the specific arrangement of posts within a channel to precisely control the trajectory of and facilitate separation of particles larger and smaller than a critical diameter (D_c). Each succeeding row within a constriction is shifted laterally at a set distance from the predecessor, this leads to the creation of separate flow laminae which follow known paths through the device. The separation mechanism of DLD works in that if the center of a particle is out with the width of the first streamline, no diffusion involved, because of the unbalanced shear stress (or due to DEP force) between the top and bottom area of the particle, it then becomes displaced into the second streamline when negotiating a post. This action continues each time such a particle passes a post, when the particle size is larger than D_c, which is called the displacement mode (we can also say the particle is locked in a single array). Meanwhile, particles that are smaller than D_c remain centered within the first streamline and follow the defined route of this streamline through the device, which is called zigzag mode (Fig. 8). Particles smaller and larger than D_c will then be separated from one another along the length of a device.

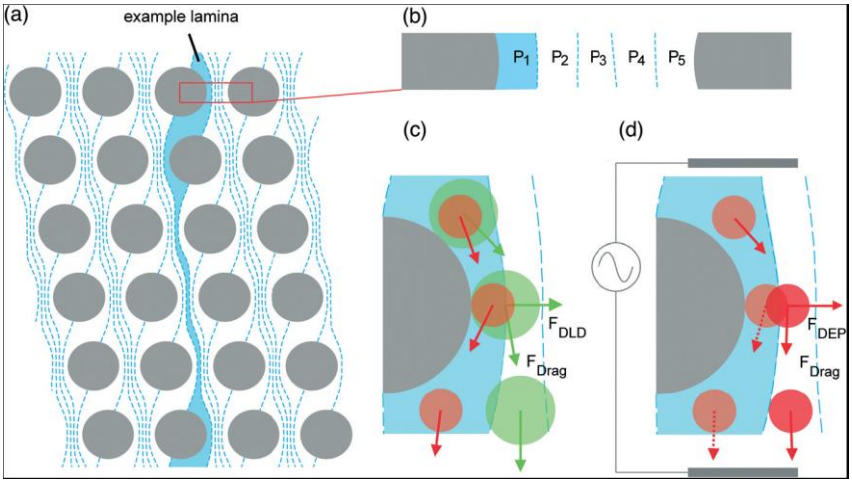

Fig. 7 The streamline orientation and basic principle of DLD with and without an external force. (A) The orientation of flow lamina induced as a consequence of lateral row shifting in a device with N = 5. (B) Position of fluid streamlines (P1, P2, P3…) between two pillars. (C) The normal motion of particles in a DLD; particles smaller than D_c (red) remain within the first streamline influenced by drag force (F_{Drag}) and continue through the device in a zigzag mode according to the path highlighted by the example lamina. Particles that are larger than D_c (green) are continually displaced into the next streamline at each successive pillar, thus facilitating particle separation. As two particles traverse the length of the device, the distance between them becomes larger. (D) When negative dielectrophoresis is induced in polarizable particles nominally smaller than D_c, they move away from the insulating posts due to dielectrophoretic force (F_{DEP}) and act as if they were larger than D_c, thus entering displacement mode. (Reprinted from 2)

Some concepts for the DLD device: 1. Forcing angle α is the angle between a column of obstacles in the lattice and the average flow (or external force), 2. Migration angle θ is the angle at which the particles migrate on average, also measured with respect to a column in the array (see figure 7). The simulations showed that, as the forcing angle increases from zero, all the particles remain *locked* to move alongside a column of obstacles in the array, i.e. $\theta = \alpha$, until the forcing angle reaches a critical value, α_c, defined as the largest forcing angle for which the particles are locked to move in the [1,0] direction (along a column of the array), which depends on particle size. Then, for each particle size, when the forcing angle is larger than their critical angle, the particles are able to move across

columns of obstacles, resulting in a periodic zigzag motion, in other words, for each forcing angle α, there is a critical diameter D_c, when the particle size is larger than D_c, the particle will migrate in displacement mode, otherwise, the particle will migrate in zigzag mode. In fact, for any forcing angle, the motion of the particles is periodic and the average migration is always along a lattice direction.

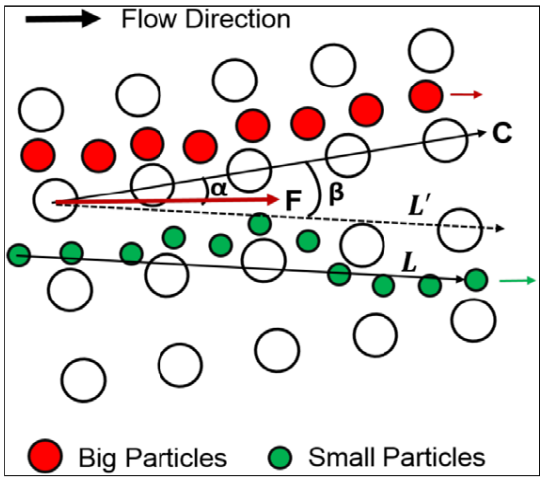

Fig 8. Schematic view of a DLD separation system. The large (small) solid circles represent the position of a large (small) particle at increasing times. The open circles represent the cylindrical obstacles. The solid line L denotes the direction of particle migration, the arrow F represents the direction of the flow and the solid line C connects centers of obstacles aligned in a lattice *column*. The forcing angle (α) is the angle of the average flow (line F) with respect to a column in the array (line C). The dashed line L' is parallel to L and illustrates the migration angle θ ($\theta=\beta-\alpha$) of the small particles. (Reprinted from 70)

1.3.2 Literature review on DLD device

The deterministic lateral displacement (DLD) was first reported by Huang et al. in 2004 to separate particles on the basis of size in continuous flow with a resolution of down to 10 nm[42]. Huang experimentally proved particle separation based on size shown in Figure 9. Since invention, this technique has been used to separate millimeter[43], micrometer[44-48]

and even sub sized particles and has been applied to diverse purposes, although mostly medical related (separation of trypanosomes[49], whiteblood cells (WBCs)[47], circulating tumor cells (CTCs)[50-52] or platelets[53] from blood for instance). To extend the range of potential applications, the specific arrangement of geometric features in DLD has also been adapted and/or coupled with external forces, e.g. acoustic[16], electric[17,18], gravitational[19] to separate particles on the basis of other properties than size such as the shape, deformability and dielectric properties of particles.

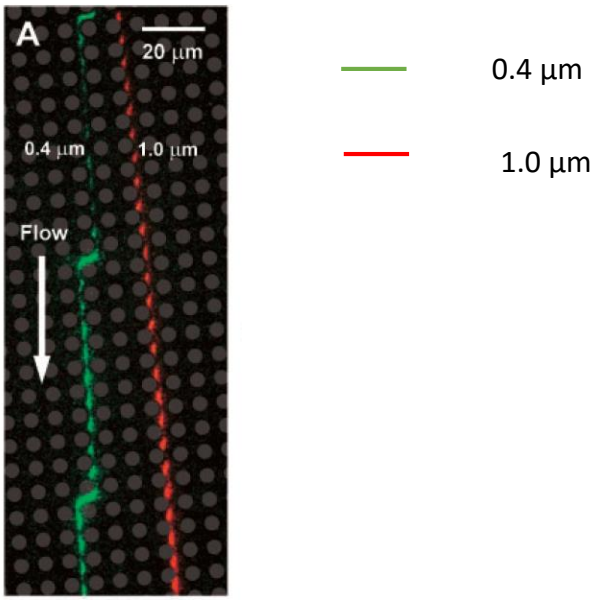

Fig 9. Particle separation by size in experiment in pressure driven DLD by Huang et al.

The separation and enrichment of micro-particles of interest is one of the main applications for DEP systems; where bioanalytical and clinical assessments, such as the manipulation of cells and biomolecules, are particularly attractive. A key aspect of DEP is the generation of a non-uniform electric field, which can be achieved in several ways. Electrode-based and insulator-based DEP (e-DEP and i-DEP, respectively) are the most

common approaches. Simultaneous sorting and enrichment of a wide variety of cells using i-DEP systems have been demonstrated earlier. Lapizco-Encinas used glass devices with arrays of circular posts and DC voltages to concentrate and separate binary mixtures of four species of bacteria (*E. coli, B. subtilis, B. cereus* and *B. megateriμm*)[54]. The simultaneous enrichment and separation of *E. coli* and *S. cerevisiae* cell in less than two minutes, employing DC potentials and devices made from glass, was reported by Moncada-Hernández and Lapizco-Encinas[55]. Pysher and Hayes developed a PDMS device with a converging sawtooth channel for the simultaneous enrichment and separation of *B. subtilis, E. coli* and *S. epidermis* cells[56]. Later, Kang showed the continuous separation of human white blood cells and breast cancer cells using a microchannel with an insulating hurdle[57]. Although many applications i-DEP systems have been focused on manipulating cells, i-DEP has also been successfully applied for the manipulation of proteins[58-60], DNA[61,62], organelles[63] and virus[64,65]. While DC fields have been traditionally used, recent studies report the application of DC-biased AC or cyclical electric fields[66-68]. For instance, Gencoglu used a DC-biased, low frequency AC field to concentrate and selectively release particles and cells from an i-DEP device with diamond-shaped insulating posts[66].

1.4 Overview of thesis

This thesis consisting of five chapters will use ALE numerical method to achieve our objectives to prove the capability particle separation of e-DLD devices. Chapter two establishes a framework for the thesis by elaborating upon the numerical methods for the two dimensional model. Governing equations, boundary conditions and material

properties used for the simulation are discussed, and grid independent study of the model is carried. Chapter three presents the parametric study of a few important factors which affect the separation of particles. The optimum parameters of the device are proposed for a higher separation efficiency. Post shape and particle shape effect are also discussed. Comparison of e-DLD with pressure-driven DLD demonstrates the advantages of using electrokinetic flow. In chapter four, key contributions of this thesis are summarized, and several future works stemming from this thesis project are proposed.

CHAPTER TWO

THEORY AND METHODS

In this section, we present 2D equations for coupled electric field and flow transport involved in the computational domain for channel under consideration is described along with boundary conditions necessary for solving the governing equations. Then we use non-dimensional the governing equations and boundary conditions to simplify the model we build. Next, we present the numerical method of Arbitrary Lagrangian Eulerian (ALE) and Lagrangian Tracking Method. Finally, we present the grid independent study to prove the feasibility of the model.

2.1 Mathematical model

2.1.1 Computational Domain

Figure 2 shows a two-dimensional (2D) model of a circular particle transport in a straight microchannel. The microchannel is 2.5 mm long and 1 mm wide with 8*6 posts in the center of the domain. The posts are 50μm in diameter, and have center to center distance of 100μm. The computational domain Ω is surrounded by the boundary ABCD and Γ (also the posts). The segments AB and CD are the inlet and the outlet, respectively, between which a pressure difference may be applied (If it is a pressure-driven flow). The segments BC and AD are the channel walls. Γ is the particle surface, which is initially located in the upstream straight section. The width of the channel is denoted as W, the length of the channel is denoted as L. The particle and channel walls are rigid, and the

fluid in the computational domain Ω is incompressible and Newtonian. The effects of Brownian motion and gravity are ignored.

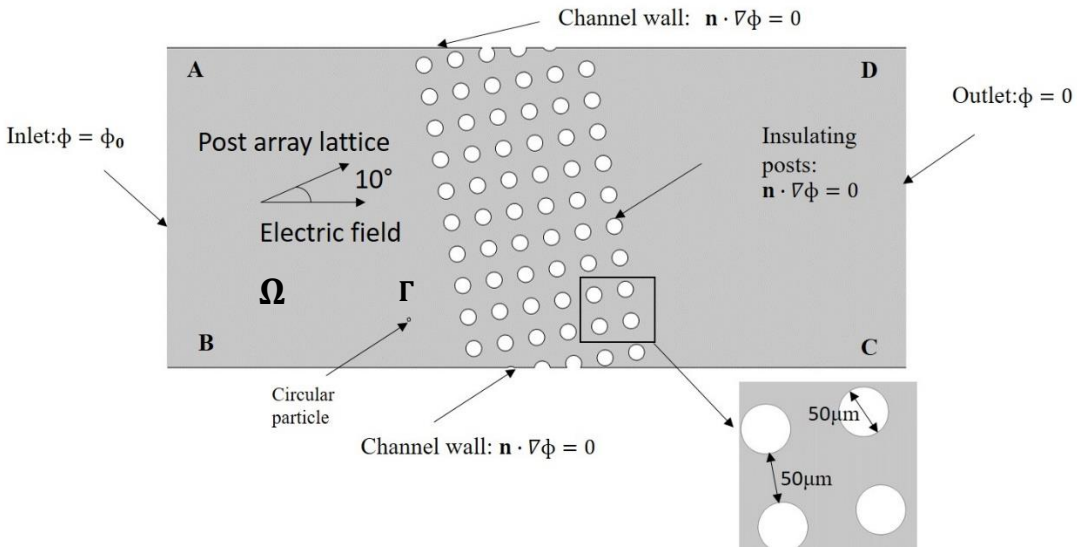

Fig 10. Computational domain used for numerical simulation

2.1.2 Governing Equations and Boundary Conditions

2.1.2.1 Governing equations for pressure-driven flow

Flow field

The conservations of fluid mass and momentum are described by the continuity equation and the Navier–Stokes (NS) equations:

$$\rho\left(\frac{\partial \mathbf{u}}{\partial t} + \boldsymbol{u} \cdot \nabla \boldsymbol{u}\right) - \mu\nabla^2\mathbf{u} + \nabla p = 0 \qquad \text{in } \Omega \tag{15}$$

$$\nabla \cdot \mathbf{u} = \mathbf{0} \qquad \text{in } \Omega. \tag{16}$$

Where **u** is the fluid velocity vector and p is the pressure, ρ and μ are the density and dynamic viscosity of the fluid, respectively, and the t is the time. Both the fluid velocity

and the pressure are initially zero in the computational domain. The pressure at the inlet and the outlet are both zero so there is no pressure imposed.

A pressure difference ΔP is imposed between the inlet AB and the outlet CD. The effect of streaming potential field on the particle transport is generally low[69], and so the electrophoretic motion of the suspended particle is ignored. The no-slip condition is applied on the channel walls ABCD and posts walls. Since the particle translates and rotates simultaneously, the boundary condition or the fluid on the particle surface contains both translational velocity and rotational velocity:

$$\boldsymbol{u} = \mathbf{U}_\mathrm{p} + \boldsymbol{\omega}_\mathrm{p} \times \left(\mathbf{x}_\mathrm{s} - \mathbf{x}_\mathrm{p}\right) \quad \text{on } \Gamma. \tag{17}$$

The particle's translational velocity is governed by the Newton's second law:

$$\mathrm{m_p} \frac{\mathrm{d}\mathbf{U}_\mathrm{p}}{\mathrm{dt}} = \mathbf{F}_\mathrm{net} \tag{18}$$

Where $\mathrm{m_p}$ is the mass of the particle, and $\mathbf{F}_\mathrm{net}$ is the net force acting on it, the net force $\mathbf{F}_\mathrm{net}$ only includes the hydrodynamic force due to the flow field:

$$\mathbf{F}_\mathrm{net=}\mathbf{F}_\mathrm{H} = \int \mathbf{T}^\mathrm{H} \cdot \mathbf{n} \mathrm{d}\Gamma = \int [-\mathrm{p}\mathbf{I} + \mu(\nabla \mathbf{u} + \nabla \mathbf{u}^\mathrm{T})] \cdot \mathbf{n} \mathrm{d}\Gamma \tag{19}$$

In this equation, $\mathbf{T}^\mathrm{H}$ is the hydrodynamic stress tensors, **n** is the unit outward normal vector, and **I** is the identity tensor.

The rotational velocity of the particle is governed by

$$\mathbf{I_p} \frac{\mathrm{d}\boldsymbol{\omega}_\mathrm{p}}{\mathrm{dt}} = \mathbf{T} = \int \left(\mathbf{x}_\mathrm{s} - \mathbf{x}_\mathrm{p}\right) \times (\mathbf{T}^\mathrm{H} \cdot \mathbf{n}) \, \mathrm{d}\Gamma, \tag{20}$$

Where $\mathbf{I_p}$ is the moment of inertia of the particle, $\mathbf{T}$ is the torque exerted on the particle by the flow field, and the right-hand side of Equation (12) is the net torque exerted on the particle.

The center $\mathbf{x}_p$ and the orientation θ_p of the particle are expressed by

$$\mathbf{x}_p = \mathbf{x}_{p0} + \int_0^t \mathbf{U}_p dt \,. \tag{21}$$

and

$$\theta_p = \theta_{p0} + \int_0^t \boldsymbol{\omega}_p dt \,. \tag{22}$$

where x_{p0} and θ_{p0} denote, respectively, the initial position and orientation of the particle.

The equation of particle motion for force and torque are, respectively:

$$m_p \frac{d\mathbf{U}_p}{dt} = \int (\mathbf{T}^H \cdot \mathbf{n})\, d\Gamma, \tag{23}$$

$$I_p \frac{d\boldsymbol{\omega}_p}{dt} = \int (\mathbf{x}_s - \mathbf{x}_p) \times (\mathbf{T}^H \cdot \mathbf{n})\, d\Gamma \,. \tag{24}$$

2.1.2.2 Governing equations for electrokinetic flow

A. Electric field

The thickness of the EDL formed adjacent to the charged surface is in the order of several nanometers, which is much smaller than the particle radius and the width of microchannel. As a result, a thin EDL approximation is adopted in the present study, which renders a zero net charge density in the fluid domain[31]. Under the thin EDL approximation, the electric field outside the EDL (Electric Double Layer) is governed by the Laplace equation:

$\nabla^2\phi=0.$ In Ω. (25)

where ϕ is the electric potential.

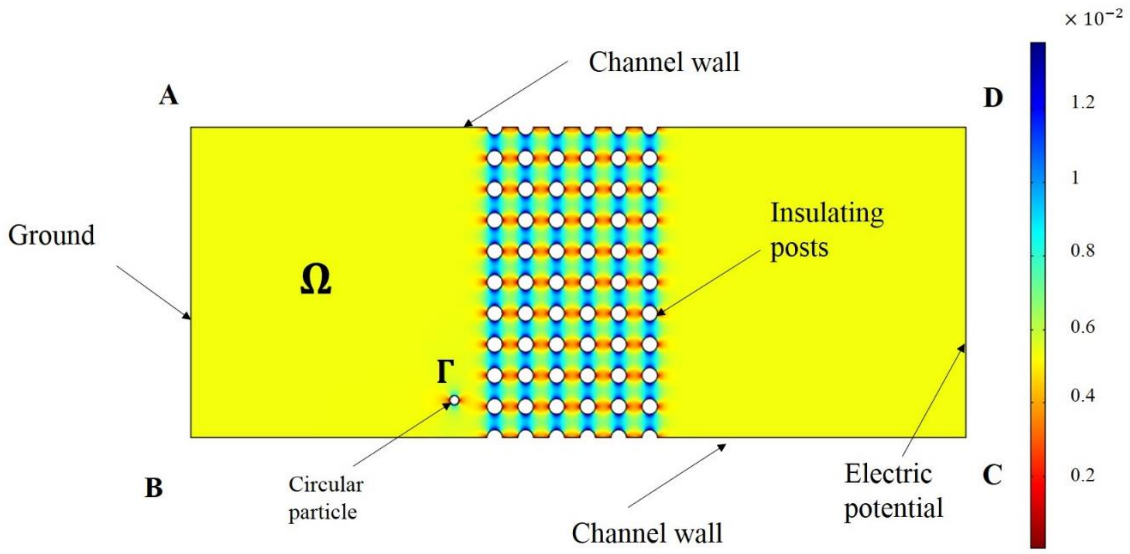

Fig 11. Electric field distribution in computational domain

B. Flow field

In the thin EDL approximation, the net charge outside the EDL is zero, which leads to a zero electrostatic body force. In addition, the Reynolds number of the electrokinetic flow in the microchannel is very low (typically lower than 0.01). As a result, the fluid motion can be modeled by the Stokes equations without any electrostatic body force, described as:

$$\rho\frac{\partial \mathbf{u}}{\partial t} - \mu\nabla^2\mathbf{u} + \nabla p = 0 \qquad \text{in } \Omega. \tag{26}$$

$$\nabla \cdot \mathbf{u} = \mathbf{0} \qquad \text{in } \Omega. \tag{27}$$

Where **u** is the fluid velocity vector and p is the pressure. Both the fluid velocity and the pressure are initially zero in the computational domain. The pressure at the inlet and the outlet are both zero so there is no pressure imposed.

The particle's translational velocity is governed by the Newton's second law:

$$m_p \frac{d\mathbf{U}_p}{dt} = \mathbf{F}_{net}, \tag{28}$$

Where m_p is the mass of the particle, and $\mathbf{F}_{net}$ is the net force acting on it. The Coulomb force arising from the charges on the particle surface exactly cancels the hydrodynamic force due to the flow field with in the EDL. Therefore, the net force $\mathbf{F}_{net}$ includes the hydrodynamic force due to the flow field originating in the outer region of the EDL, and the DC DEP force $\mathbf{F}_{DEP}$ arising from the interaction between the dielectric particle and the spatially non-uniform electric field:

$$\mathbf{F}_H = \int \mathbf{T}^H \cdot \mathbf{n} d\Gamma = \int [-p\mathbf{I} + \mu(\nabla \mathbf{u} + \nabla \mathbf{u}^T)] \cdot \mathbf{n} d\Gamma, \tag{29}$$

$$\mathbf{F}_{DEP} = \int \mathbf{T}^E \cdot \mathbf{n} d\Gamma = \int \varepsilon_0 \varepsilon_f \left[\mathbf{EE} - \frac{1}{2}(\mathbf{E} \cdot \mathbf{E})\mathbf{I}\right] \cdot \mathbf{n} d\Gamma \, . \tag{30}$$

In these equations, $\mathbf{T}^H$ and $\mathbf{T}^E$ are, respectively, the hydrodynamic and Maxwell stress tensors. **E** is the electric field related to the electric potential by $\mathbf{E}=-\nabla\phi$. The integration of the first term of the integrand in the right-hand side of Equation (11) vanishes due to Equation (4), which renders the integration of the Maxwell stress tensor as the pure DEP force.

The rotational velocity of the particle is determined by

$$\mathbf{I_p}\frac{\mathrm{d}\boldsymbol{\omega}_\mathrm{p}}{\mathrm{dt}} = \int(\mathbf{x}_\mathrm{s}-\mathbf{x}_\mathrm{p}) \times (\mathbf{T}^\mathrm{H}\cdot\mathbf{n} + \mathbf{T}^\mathrm{E}\cdot\mathbf{n})\,\mathrm{d}\Gamma, \tag{31}$$

Where $\mathbf{I_p}$ is the moment of inertia of the particle, and the right-hand side of Equation (12) is the net torque exerted on the particle.

The center $\mathbf{x}_\mathrm{p}$ and the orientation θ_p of the particle are expressed by

$$\mathbf{x}_\mathrm{p} = \mathbf{x}_{\mathrm{p}0} + \int_0^\mathrm{t}\mathbf{U}_\mathrm{p}\mathrm{dt}\,. \tag{32}$$

and

$$\theta_\mathrm{p} = \theta_{\mathrm{p}0} + \int_0^\mathrm{t}\boldsymbol{\omega}_\mathrm{p}\mathrm{dt}\,. \tag{33}$$

where x_{p0} and θ_{p0} denote, respectively, the initial position and orientation of the particle.

The equation of particle motion for force and torque are, respectively:

$$\mathrm{m_p}\frac{\mathrm{d}\mathbf{U}_\mathrm{p}}{\mathrm{dt}} = \int(\mathbf{T}^\mathrm{H}\cdot\mathbf{n} + \mathbf{T}^\mathrm{E}\cdot\mathbf{n})\,\mathrm{d}\Gamma\,, \tag{34}$$

$$\mathrm{I_p}\frac{\mathrm{d}\boldsymbol{\omega}_\mathrm{p}}{\mathrm{dt}} = \int(\mathbf{x}_\mathrm{s}-\mathbf{x}_\mathrm{p}) \times (\mathbf{T}^\mathrm{H}\cdot\mathbf{n} + \mathbf{T}^\mathrm{E}\cdot\mathbf{n})\,\mathrm{d}\Gamma\,. \tag{35}$$

2.1.2.3 Boundary Conditions

Boundary conditions required to solve the coupled equations except for the symmetry ones are summarized below.

A. Electric field

1) The electric potentials applied on the inlet and outlet are, respectively:

$$\phi = 0 \qquad \text{on the inlet.} \tag{36}$$

$\phi = \phi_0$ on the outlet. (37)

2) All the other rigid surfaces are electrically insulating:

$\mathbf{n} \cdot \nabla\phi = 0$ on AC and BD. (38)

where **n** is the unit normal vector pointing from the boundary surface into the fluid.

B. Flow field

A normal flow with zero pressure is specified at the inlet and outlet of the fluid domain as mentioned before. Since the rigid wall is charged, an electroosmotic flow (EOF) is governed next to the charged boundary, which is approximated by the Smoluckowski slip velocity in the present study owing to the EDL. Therefore, the EOF fluid velocity on the channel wall and the post wall is

$$\boldsymbol{u} = \frac{\varepsilon_0 \varepsilon_f \zeta_w}{\mu} (\mathbf{I} - \mathbf{nn}) \cdot \nabla\phi \quad \text{on the channel wall and post wall.} \tag{39}$$

where ε_0 is the permittivity of the vacuum, ε_f is the permittivity of the fluid. ζ_w is the zeta potential of the channel wall. The quantity $(\mathbf{I} - \mathbf{nn}) \cdot \nabla\phi$ defines the electric field tangential to the charged surface, with **I** denoting the second order unit tensor[51].

As the particle translates and rotates, the fluid velocity in the particle surface includes the translational velocity $\mathbf{U}_p$, rotational velocity ω_p, and Smoluckowski slip velocity addressing the induced EOF:

$$\boldsymbol{u} = \frac{\varepsilon_0 \varepsilon_f \zeta_p}{\mu} (\mathbf{I} - \mathbf{nn}) \cdot \nabla\phi + \mathbf{U}_p + \omega_p \times \left(\mathbf{x}_s - \mathbf{x}_p\right) \text{ on particle surface.} \tag{40}$$

In this equation, ζ_p is the zeta potential of the particle, $\mathbf{x}_s$ and $\mathbf{x}_p$ are, respectively, the position vector of the surface and the center of the particle.

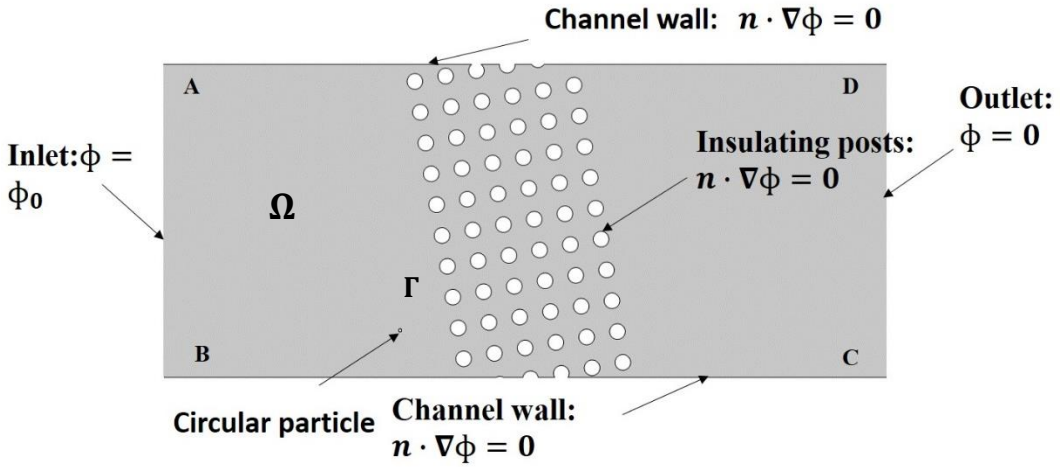

Fig 12. Boundary conditions in computational domain

2.1.3 Dimensionless Analysis of Governing Equations

The particle radius r, as the length scale; the electric potential on segment CD ϕ_{CD}, as the potential scale; $U_c = \varepsilon_0 \varepsilon_f \zeta_p \phi_0/(\mu \cdot r)$ as the velocity scale; and $\mu U_0/r$ as the pressure scale are selected to normalize all the previous governing equations:

$$\nabla^{*2}\phi^* = 0 \qquad \text{in } \Omega. \tag{41}$$

$$\mathrm{Re}\frac{\partial \mathbf{u}^*}{\partial t^*} - \nabla^{*2}\mathbf{u}^* + \nabla^* p^* = 0 \qquad \text{in } \Omega. \tag{42}$$

$$\nabla^* \cdot \mathbf{u}^* = \mathbf{0} \qquad \text{in } \Omega. \tag{43}$$

And also the corresponding boundary conditions,

$$\mathbf{n} \cdot \nabla^*\phi^* = 0 \qquad \text{on AC and BD.} \tag{44}$$

$$\phi^* = 1 \qquad \text{on CD.} \tag{45}$$

$$\boldsymbol{u}^* = \gamma(\mathbf{I} - \mathbf{nn}) \cdot \nabla^* \phi^* \qquad \text{on the channel wall and posts.} \tag{46}$$

$$\boldsymbol{u}^* = (\mathbf{I} - \mathbf{nn}) \cdot \nabla^* \phi^* + \mathbf{U}_p{}^* + \omega_p{}^* \times \left(\mathbf{x}_s{}^* - \mathbf{x}_p{}^*\right) \text{ on particle surface.} \tag{47}$$

In this equations, $\mathrm{Re} = \rho U_c r/\mu$, and $\gamma = \zeta_w/\zeta_p$ is the ratio of the zeta potential of the particle to that of the channel wall.

The force and torque are, respectively, normalized by μU_c and $\mu r U_c$, yielding the dimensionless equation of the particle motion:

$$m_p{}^* \frac{d\mathbf{U}_p{}^*}{dt^*} = \int (\mathbf{T}^{H*} \cdot \mathbf{n} + \mathbf{T}^{E*} \cdot \mathbf{n})\, d\Gamma^*, \tag{48}$$

$$I_p{}^* \frac{d\boldsymbol{\omega}_p{}^*}{dt^*} = \frac{\phi_0}{\zeta_p} \int \left(\mathbf{x}_s{}^* - \mathbf{x}_p{}^*\right) \times (\mathbf{T}^{H*} \cdot \mathbf{n} + \mathbf{T}^{E*} \cdot \mathbf{n})\, d\Gamma^* . \tag{49}$$

Where the mass and the moment of the inertia are, respectively, normalized by $r\mu/U_c$ and $r^3\mu/U_c$,

$$T^{H*} = -p^* \mathbf{I} + (\nabla^* \mathbf{u}^* + \nabla^* \mathbf{u}^{*T}) , \tag{50}$$

and

$$T^{E*} = \mathbf{E}^* \mathbf{E}^* - \frac{1}{2}(\mathbf{E}^* \cdot \mathbf{E}^*)\mathbf{I} . \tag{51}$$

2.2 Numerical Methods

2.2.1 Arbitrary Lagrangian Eulerian (ALE) Method

In this thesis, a numerical model of e-DLD (which belongs to i-DEP system) is developed to simultaneously solve the electric field, flow field in order to separate particles with several different properties, using an Arbitrary Lagrangian-Eulerian (ALE) method, which is regarded as one of the most efficient computational approaches to deal with moving boundaries in the computational domain. The proposed numerical model without considering the particle deformation has already been successfully implemented to simulate the pressure-driven[71], and electrokinetic motion[72-76] of rigid particles in micro-channels, indicating good agreements with experimental results. The study of DEP effect on a deformable particle was also published[77].

Commercial finite element software package, COMSOL Multiphysics 4.4 (Burlington, MA) was used to carryout numerical simulations. 'Electrical currents', 'Moving Mesh', and 'Creeping flow' interfaces were coupled together to solve for the governing equations using the predefined ALE method, which tracks the particle motion in a Lagrangian fashion and at the same time solves the fluid flow and the electric field in a Eulerian framework. Here, the Eulerian reference frame and the Lagrangian reference frame are fixed to the spatial space and the computational mesh, respectively. The computational domain Ω in Fig. 6 is discretized into quadratic triangular elements with a higher concentration of elements around the particle surface and the posts.

Briefly, the ALE method updates the particle's location and orientation by deforming the mesh after each computational time step using. As the particle translates and rotates, the

mesh becomes highly deformed, which could affect the accuracy of the numerical results. Therefore, we usually assign a minimum mesh quality level below which the mesh deformation is forced to stop. A new geometry is then generated on the new geometry to continue the computational until the next remesh step.

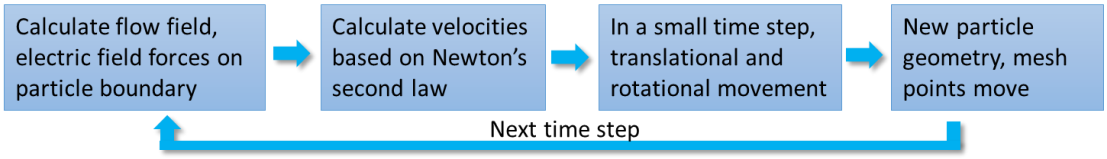

Fig 13. Process of using ALE methods to track particle motion

In our simulation, there will be a highly deformed domain (we call it physical domain) which changes with time and very hard to work with. Instead of solving this domain, we can use a linear map to transform the physical domain to a reference domain which is fixed in time and very easy to work with. We can first calculate the data from a fixed point X in reference domain. Then we can use the inverse of the previous linear map to transform back to the corresponding point x at physical domain, and get the data of this point. In this way, it is much easier to calculate the data form a deformed domain.

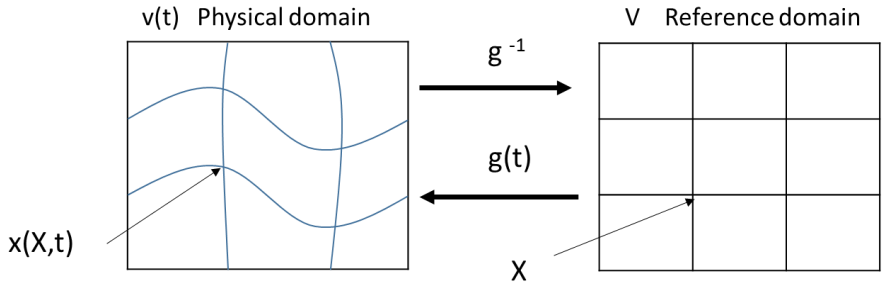

Fig 14. Process of using ALE methods to solve time-dependent deformed domain

The 2D geometry was created using the 'Geometry' feature of COMSOL. The domain was meshed using free triangular elements and the entire domain had approximately 120,000 number of mesh elements. The model was solved by using a nonlinear, segregated, iterative solver with appropriate damping factors to achieve a faster convergence.

The parameters we use in the simulation and material properties are listed in the table below:

TABLE 1. Summary of parameters and material properties used for modelling

Symbol	Value or Expression	Unit	Description
ζ_w	-50	mV	Zeta potential of wall
ζ_p	-80	mV	Zeta potential of particle
ρ	1000	kg/m^3	Fluid mass density
eps_r	80	1	Relative permittivity of fluid
eps0	8.854e-12	F/m	Permittivity of vacuum
Xp0	-35	μm	Initial x location of particle
Yp0	-45	μm	Initial y location of particle
Masss	$\rho * pi * r^2$	kg	Dimensional particle mass
Mass	$Masss * \frac{U_c}{\mu}/r$	1	Dimensionless particle mass
Ir	$\frac{1}{2} * Masss * r^2 * \frac{U_c}{\mu}/r^3$	1	Dimensionless moment of inertia
r	10e-6	m	Particle radius
zetar	2.06	1	Zeta potential ratio
ep	32e-3	V	Zeta potential of particle

μ	1e-3	pa*s	Fluid viscosity
U_c	eps_r*eps0*ep*v0/(μ*r)	m/s	Velocity scale
v0	50	V	Applied voltage
Re	$\rho*U_c*r/\mu$	1	Reynolds number
depr	V0/ep	1	DEP force coefficient

In the simulation of particle trajectory, important assumptions are made as follows[32]:

1) The thermo-physical properties of the liquid are constant, which means the thermal conductivity of the fluid is assumed constant;
2) No thermal effect on flow field and particle velocity;
3) The particle and the channel walls are non-porous, and not reacting with the surrounding liquid;
4) The thickness of the EDL next to the channel wall and the particle surface are very small compared to the particle size;
5) The effect of the surface conductance on the EDL is negligible;
6) The rotation of the particle does not affect the particle's translational motion;
7) Creeping flow, i.e., Re<<1;

2.2.2 Lagrangian Tracking Method

To simplify the analysis, a simplified model based on Lagrangian tracking method is used to predict the particle motion. We get the expression by electrokinetic mobility and EDP mobility based on point dipole method. In this method, only the effect of the flow and the

electric field on the particle is considered, whereas the effect of the particle on the flow and the electric field is neglected, or a correction factor can be introduced to account for the particle size effects on the DEP force and is determined by fitting the numerical predictions to the experimental data. Since the particle sizes are small compared to the dimension of the channel we are using, this assumption is acceptable. However, if the characteristic length of micro-/nanofluidic devices becomes comparable to the particle size, which renders the point dipole method inaccurate for DEP force calculation. Previous studies have demonstrated that the most rigorous approach for DEP force calculation is direct integration of Maxwell stress tensor (MST).

By balancing $\mathbf{F}_{DEP}$ with the Stokes drag force, one can get the particle dielectrophoretic velocity, $\mathbf{U}_{DEP}$, which will be superimposed to $\mathbf{U}_{EK}$. Namely, the real particle velocity of electrokinetic motion within a microchannel will be $\mathbf{U}_{P} = \mathbf{U}_{DEP} + \mathbf{U}_{EK,}$ which according to chapter one is,

$$U_P = \frac{\varepsilon_m(\zeta_p - \zeta_w)E_x}{\mu} + \frac{\varepsilon_m r^2 f_{CM}}{3\mu}\nabla E_{rms}^2 \qquad (20)$$

Where ε_m ($\varepsilon_m = \varepsilon_0\varepsilon_f$) is the absolute permittivity of the suspending medium, ζ_p is the zeta potential of the particle, ζ_w is the zeta potential of the wall, μ is the dynamic viscosity, E_x is the electric field magnitude in x direction, r is the spherical particle radius.

2.3 Grid independent study

In order to save time and get a more accurate results, we choose to set the mesh in the rectangular area which the particle might migrate be the best mesh quality, while other

area will have the worse mesh. The goal is to find an appropriate mesh quality for the rectangular area which is good enough for doing the simulation.

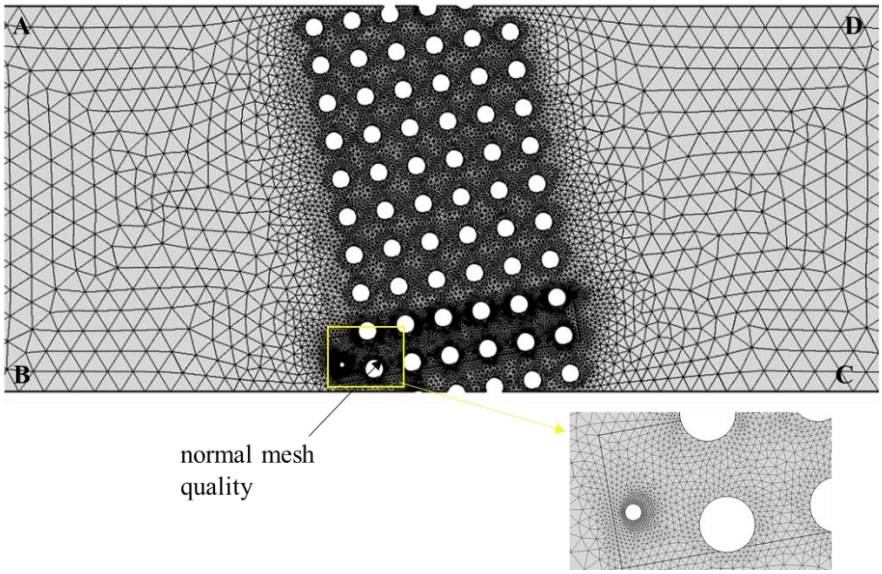

Fig 15. Mesh quality selection in computational domain

We find that using extremely fine mesh quality in the rectangular area, the domain elements are: 30886, while using normal mesh quality in the rectangular area, the domain elements are: 20469. It is clear that using normal mesh quality will save lots of space and time. The goal in this study is to prove whether using normal mesh quality is good enough to conduct the simulation process.

We use different mesh qualities in the small rectangular area in my geometry to compare the particle's trajectory. We also compare particle translational velocity (u_p and v_p) using the best mesh quality (extremely fine) with the worst mesh quality we use (normal). They almost have the same trend. We also compare the electric field magnitude of three random points in the post array area using different mesh qualities. From the results we got, the model is grid independent.

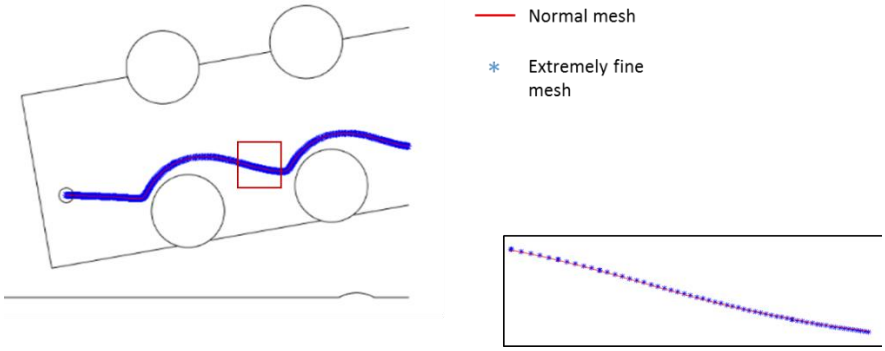

Fig 16. Trajectory comparison between extremely fine mesh quality with normal mesh quality

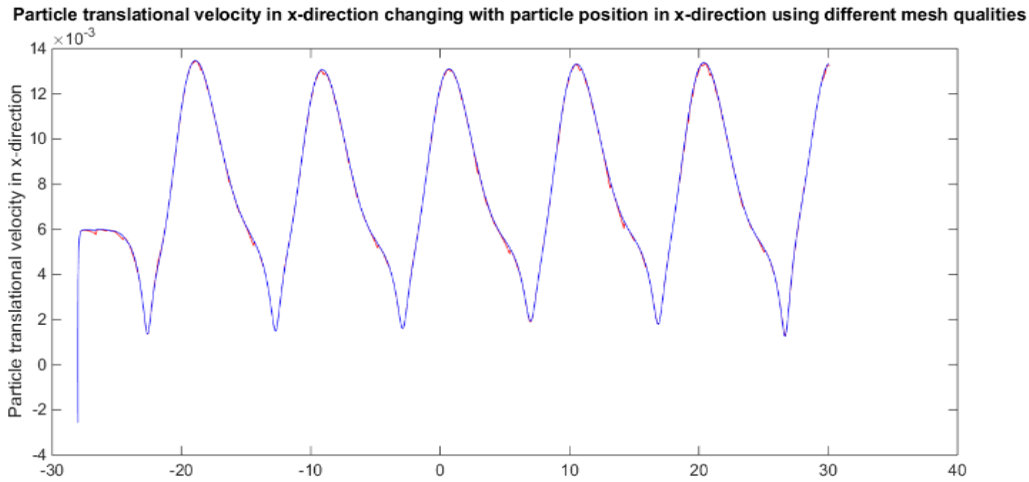

Fig.17 Translational velocity comparison between extremely fine mesh quality (blue) with normal mesh quality (red)

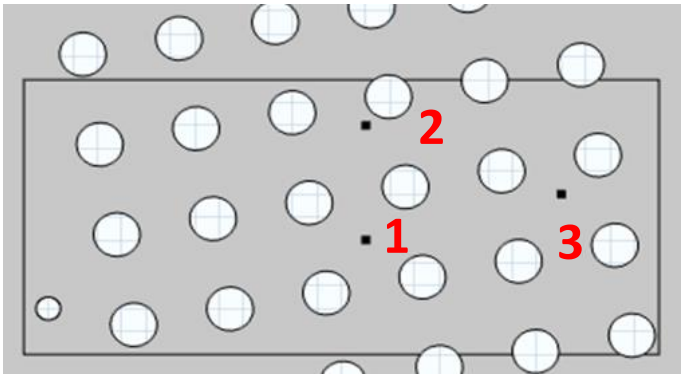

Fig 18. Three random points chosen in the geometry to verify grid independent

TABLE 2. Electric field magnitude of three random points in post area using different mesh qualities

E(norm) V/m	Extremely Fine	Extra Fine	Finer	Fine	Normal
Point 1	0.01202	0.01120	0.01201	0.01198	0.01198
Point 2	0.01078	0.01077	0.01078	0.01078	0.01078
Point 3	0.01050	0.01050	0.01050	0.01051	0.01050

From the results, it is clear that the model is grid independent. We can use normal mesh quality for the rectangular area is good enough for the simulation, and won't influence the results we got. This is the final mesh distribution we use for the e-DLD device model.

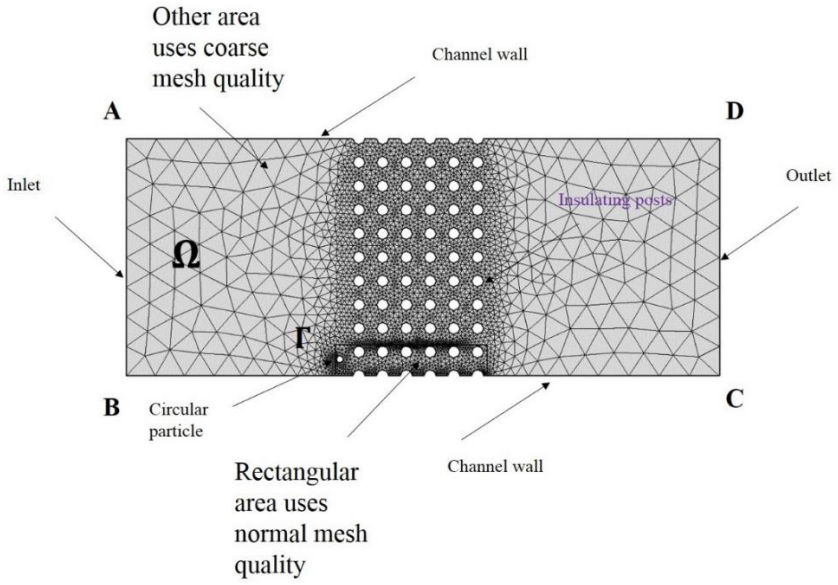

Fig 19. Mesh distribution for computational domain

CHAPTER THREE

RESULTS AND DISCUSSION

3.1 Circular particle separation by size using e-DLD device

3.1.1 Separation of 5μm, 10μm and 15μm particles

From the formula of DEP force, it is obvious that circular particles with different size will have different DEP force acting on it, the larger the particle size, the stronger DEP force acting on the particle. Therefore, the larger particle will be get locked in single array (displacement mode) easier than the smaller particle. From previous chapter, we know that the critical diameter of particle in e-DLD device is determined by the factors such as forcing angle (shift fraction), post gap ratio and the electric field. Using certain combination of these factors can separate the particle by size. Using a certain reference parameter: forcing angle α= 20°, electric field E= 30 KV/m, gap size is 50μm, and post diameter is also 50μm, we can get the separation of 5μm, 10μm and 15μm circular particles. Average migration angle (θ) difference between different particles is chosen to be the criterion of separation efficiency.

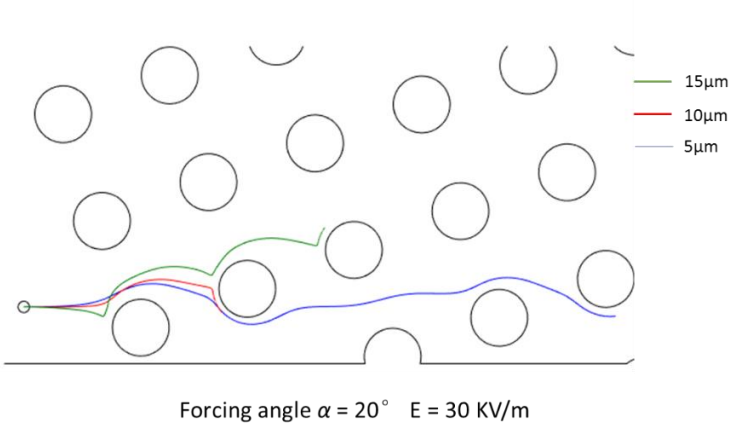

Fig 20. Separation of 5μm, 10μm and 15μm circular particles in e-DLD device

The reason different sizes of circular particles get separated is the magnitude and the direction of the electric forces (mainly DEP force) acting on the particles when they enter into the post area is different, the electric forces acting on larger particle is stronger, so that the larger particle was deflected out of its original streamline and onto the streamlines which are further from the post (Fig15 F, J). While the smaller particle may keep migrating in the same streamline all the time. Different size of circular particle will therefore migrate in different path, that's how the separation happens. Here are some figures of the key points of the separation process (The magnitude of electric forces showing is the non-dimensional value):

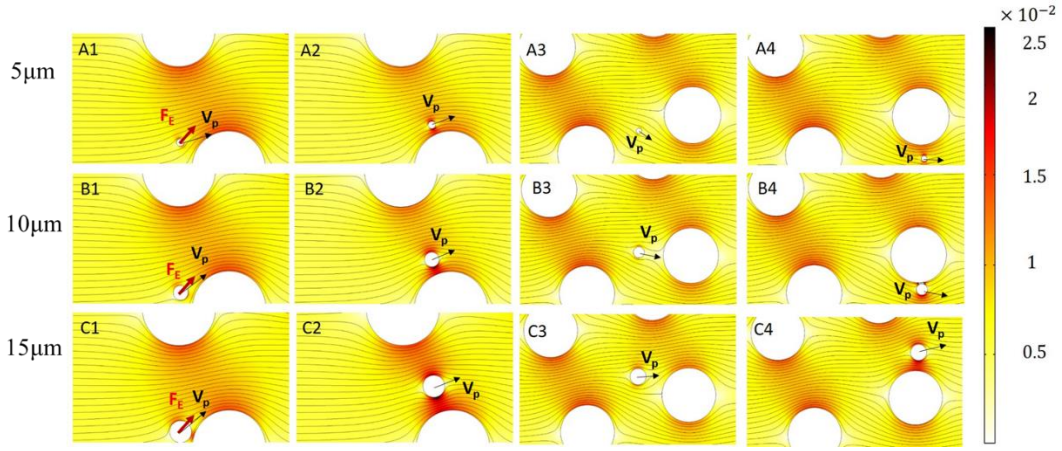

Fig 21. Migration process of 5μm, 10μm and 15μm particles at forcing angle α=20° using E=30KV/m, showing with non-dimensional electric field distribution and streamlines.

The larger particles, the larger the electric forces acting on them. Also, the vertical component of electric forces acting on different particles are clearly much different, that is why the larger particles get deflected further away from the posts than the smaller particles.

From the results and analysis above, we can conclude that using forcing angle α=20°, we can easily separate 5μm, 10μm and15μm particles since they exhibit quite different migration angles.

3.1.2 Characteristic definitions of e-DLD particle separation

In the simulation, we find that for a certain size of particles, if we increase the forcing angle from 0° to a certain value, the particle will first move follow the direction of a column of the posts ($\alpha=\theta$), that's we called the *displacement mode*. When forcing angle reaching that certain value, the particle will migrate follow the electric field ($\theta \geq 0°$, $\alpha \neq \theta$), that's we call the *zigzag mode*. Every particle's migration can be either displacement

mode or zigzag mode. Here is the plot from the simulation results of 5μm, 10μm and 15μm particles' migration angle (θ) changing with the forcing angle (α).

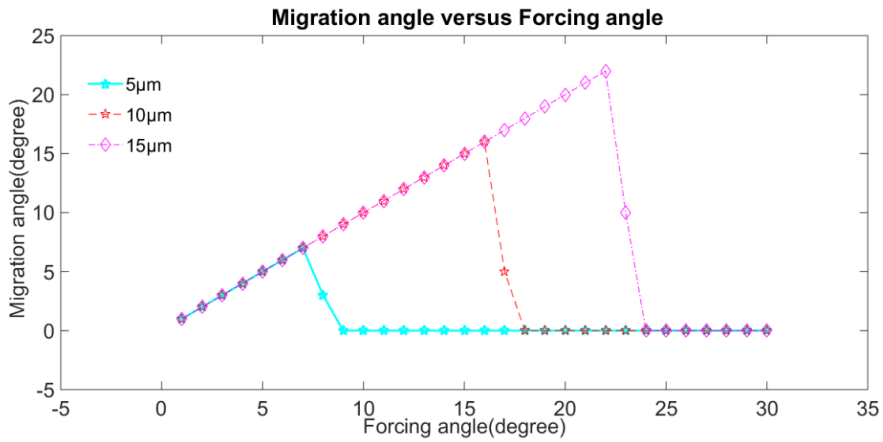

Fig 22. Migration angle (θ) as a function of forcing angle (α) for 5μm, 10μm and 15μm particles

We have performed a series of independent simulations to measure the migration angle of suspended particles of these three different sizes. They are electrokinetically driven through the obstacle array at forcing angles, α, ranging from 0° to 30°, with respect to the main lattice directions. In Figure 22, we present the migration angle, α, versus forcing angle, θ, for all particles over a range of forcing directions (0°-30°). First, we investigate the existence of a *displacement mode*, in which particles move along a column of obstacles ($\alpha=\theta$) for forcing angles lower than a certain critical angle. Then, we characterize the transition into the *zigzag mode* ($\theta \geq 0°$) as the forcing angle increases beyond the critical value. There are sharp transitions between locking directions, a phenomenon that could be harnessed to obtain high selectivity and resolution in the separation process. It is also clear that, at certain special forcing angles, particles of different size exhibit different migration angles, which is the basis for separation.

Clearly, in all cases, we observe a sharp transition from *displacement mode* (i.e. *locked mode at* $\alpha=\theta$) to *zigzag mode.* We also find that particles exhibit periodic trajectories and directional locking. That is, particles move at certain lattice directions that remain constant for a range of forcing angles. For example, all particles are locked in the [1,0] direction at small forcing angles. Essentially, particles move along a line of consecutive posts in one of the principal directions of the array (say a column of the array). Only at large enough forcing angles the particle move across a column of obstacles in the array and their migration angle becomes different from [1,0]. Interestingly, the first transition angle (or critical angle) α_c, defined as the largest forcing angle for which the particles are locked to move in the [1,0] direction (along a column of the array), shows the largest variation with the size of the particles, with smaller particles transitioning at smaller angles. More specifically, the smallest particles, 5μm, exhibit a very early transition at α~7°, while 10μm and 15μm particles remain locked to move in the [1,0] lattice direction until about α~16° and α~22°, respectively. Therefore, a driving direction α~20° would efficiently separate the 5μm particles from the 15μm ones.

3.2 Forcing angle (α) effect

Forcing angle α is the angle between the electric field and the column of the posts, at specific forcing angles, different particles migrate in different mode. Since we have already proved the separation at forcing angle α=20°, we will use forcing angle α=10° and 30° to try to implement the separation of different sizes of particles.

Here are the phenomena of different size of particles get separated at forcing angle α=10° and α=30°: at α=10°, since the DEP force is big enough to deflect 10μm and 15μm particles fur away from the posts (Fig18. F, G), all the 10μm and 15μm move in the displacement mode (locked in the single array), the 5μm particle move in zigzag mode; at α=30°, since the DEP force is not enough to deflect all particles fur away from the posts, all particles in different sizes move in the zigzag mode.

At forcing angle α=10°:

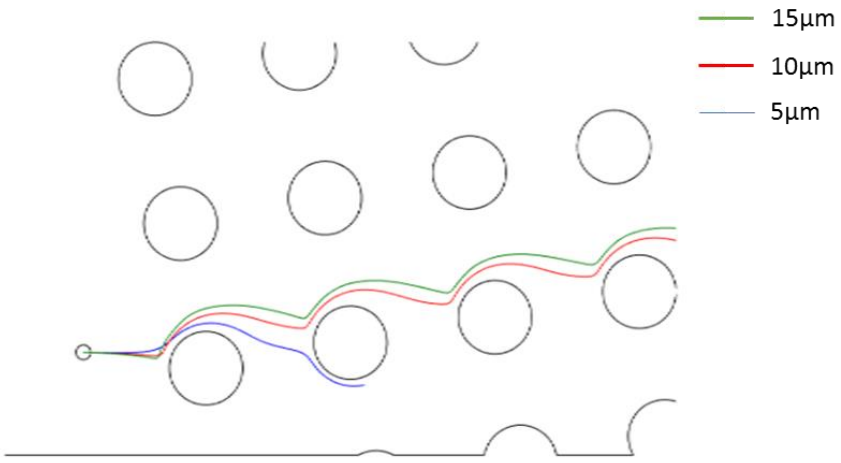

Fig 23. Separation of 5μm, 10μm and 15μm circular particles with forcing angle α=10° in e-DLD device

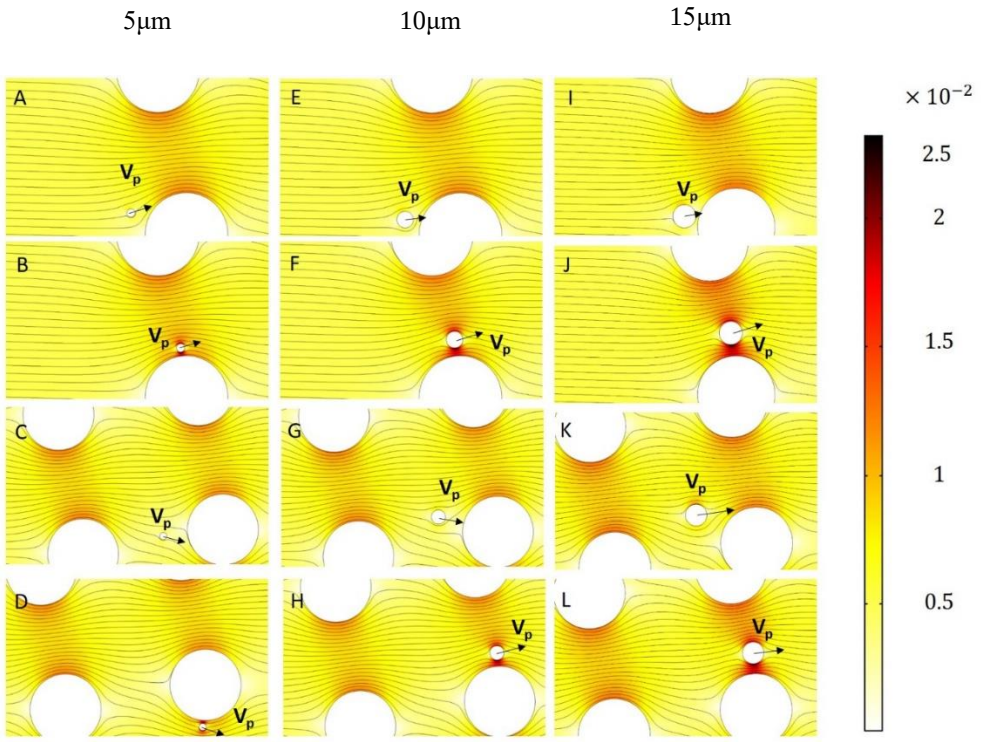

Fig 24. Migration process of 5μm, 10μm and 15μm particles at forcing angle α=10° using E=30KV/m, showing with non-dimensional electric field distribution and streamlines

At forcing angle α=30°:

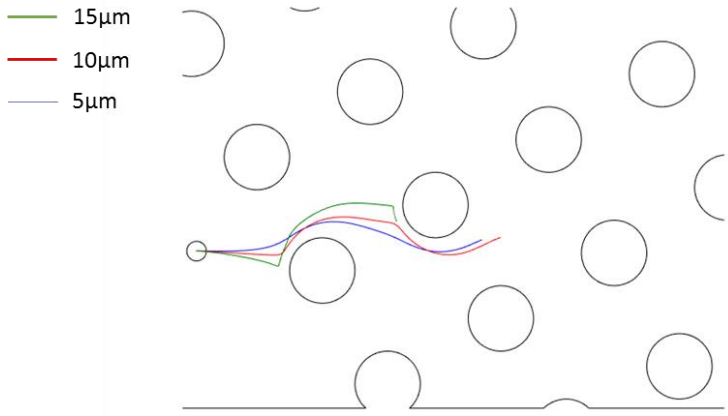

Fig 25. Separation of 5μm, 10μm and 15μm circular particles with forcing angle α=30° in e-DLD device

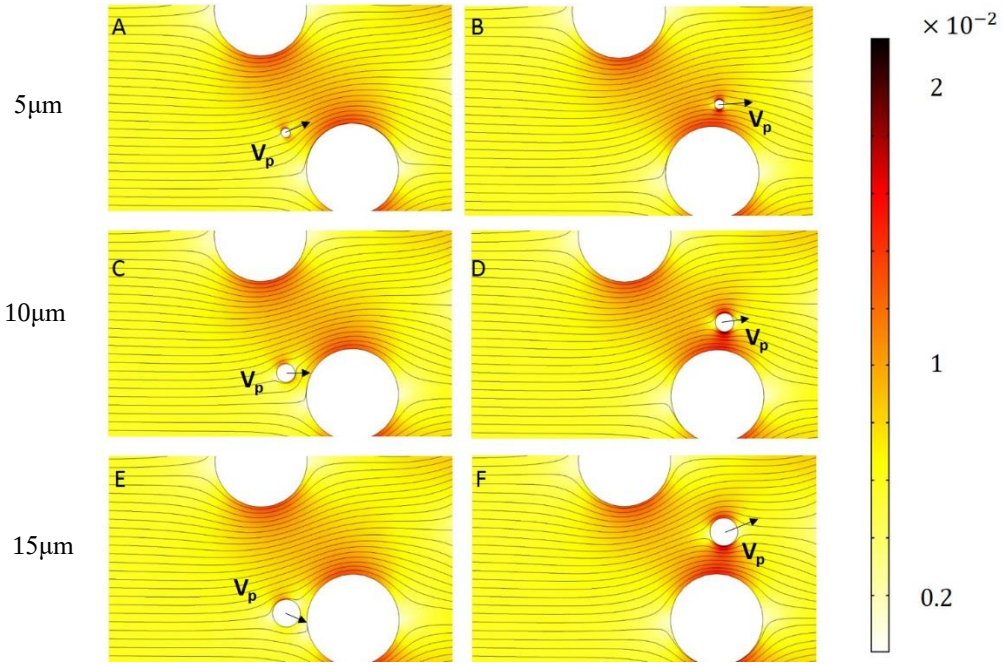

Fig 26. Migration process of 5μm, 10μm and 15μm particles at forcing angle α=30° using E=30KV/m, showing with non-dimensional electric field distribution and streamlines

After comparing the trajectories of different sizes of particles using different forcing angles, we can also think comparing certain size of particle moving at different forcing angles. If we keep all other parameters to be constant, just change the forcing angle α of the posts, the DEP force's direction will also change accordingly. As the forcing angle keep increasing, the vertical component of DEP force will decrease. For the larger particles, they will not be able to be deflected onto other streamlines, they may just follow the same streamline (zigzag mode) as the smaller particles do.

Here is a table and a plot which include three different sizes of particles' migration angle in three forcing angles we have already discussed above at electric field E= 30KV/m.

TABLE 3. Migration angles of different size of particles at different forcing angle α and at E=30KV/m

Forcing angle / Particle size	10°	20°	30°
5μm	0°	0°	0°
10μm	10°	0°	0°
15μm	10°	20°	0°

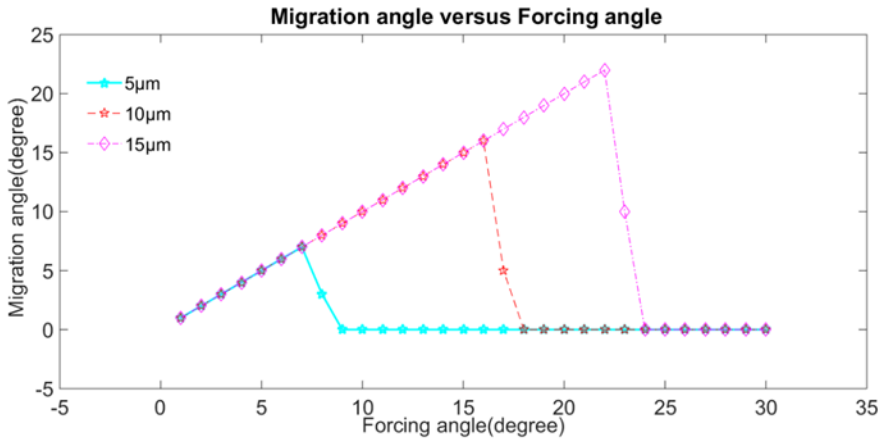

Fig 27. Migration angles for 5, 10, 15μm particles using different forcing angle at 30KV/m

From the plot above, it is obvious that when θ=20°, the difference of migration angle θ between the 5μm (θ =0°), 10μm (θ =11°) and 15μm (θ=20°) particles become the biggest. It will be efficient to separate these three different sizes of particles. In other words, when E=30KV/m, the separation efficiency is the best which has the forcing angle α=20° to separate 5μm, 10μm and 15μm particles together. Moreover, if we want to separate two different sizes particles, using forcing angle α=20°, we can also get the highest separation

efficiency of 5μm (θ=0°) and 15μm (θ=20°) or 5μm (θ=0°) and 10μm (θ=11.9°) particles. Using forcing angle α=30°, we can also get the best separation efficiency of 10μm (θ=2.9°) and 15μm (θ=17.6°) particles.

3.3 Post gap ratio (D/G) effect

According to the formula of critical diameter of pressure driven flow, the critical diameter should also be influenced by gap size in electrokinetic flow. Theoretically, since the gap size will definitely influence the electric gradient. First of all, we want to make sure whether the gap size will have impact on the particle trajectory. Originally, the gap size between the posts is 50μm. Keeping the post size to be constant, let the forcing angle be 10° and use particle size 10μm. Changing the gap size to 25μm, 40μm, 75μm and 100μm and the results are as follows:

TABLE 4. The relation between the critical diameter and gap size

Gap size	Particle locked in single array?	Critical Diameter
25μm	Yes	Smaller than 10μm
40μm	Yes	Smaller than 10μm
50μm	Yes	Smaller than 10μm
75μm	No	Larger than 10μm
100μm	No	Larger than 10μm

In the original case, when the gap size is 50μm, the 10μm particle is locked in the single array (displacement mode). When using smaller gap size (25μm, 40μm), the electric gradient will be smaller in the post area, DEP force acting on particle will be stronger,

particles will be deflected further away from the posts. 10μm particle should definitely be locked in the single array (displacement mode), the results justified this relation; when using larger gap size (75μm, 100μm), the critical diameter should increase, thus, the critical diameter should be larger than that of gap size is 50μm. At larger gap size, the electric gradient will be smaller, DEP force acting on particle will be smaller. Thus using gap sizes greater than 50μm, particle may or may not be locked in the single array. The results show that when using 75μm gap size the 10μm particle is not locked in the single array (zigzag mode), and it's the same using 100μm gap size, the 10μm particle is also not locked in the single array (zigzag mode). Above all, it is clear that gap size does influence the particle trajectory. If we increase the gap size, the electric gradient will be smaller in the post areas, particle will easily migrate in zigzag mode instead of displacement mode.

Secondly, it seems the changing post size will also influence the particle trajectory by altering electric field. Originally, the post diameter is 50μm. Keeping the gap between the posts to be constant, let the forcing angle still be 10° and use particle size 10μm. Changing the post diameter to 25μm, 40μm, 75μm and 100μm, the results are as following:

TABLE 5. The relation between the critical diameter and post size

Post size	Particle locked in single array	Critical Diameter
25μm	No	Larger than 10μm
40μm	No	Larger than 10μm
50μm	Yes	Smaller than 10μm
75μm	Yes	Smaller than 10μm
100μm	Yes	Smaller than 10μm

In the original case, when the post size is 50μm, the 10μm particle is locked in the single array, at larger post sizes, the electric gradient will be larger, DEP force acting on particle will be greater, particle will thus be deflected further away from the posts. Thus using post sizes greater than 50μm, particle will be locked in the single array (displacement mode). For post sizes smaller than 50μm, the electric gradient will be smaller, DEP force will also become smaller, particle will easily move in zigzag mode instead of displacement mode. From the results we get, it is obvious that post size does influence the particle trajectory. If we increase the post size, the electric gradient will be stronger in the post areas, particle will easily migrate in displacement mode.

Finally, we will look into whether ratio of post diameter and gap size will affect the particle trajectory. Originally, the post gap ration is 1, then change the ratio to 0.5, 0.67, 0.8, 1.25, 1.5 and 2. Here are the results:

TABLE 6. The relation between the critical diameter and post gap ratio

Post gap ratio	Particle locked in single array?	Critical Diameter
0.5 (D=50μm, G=100μm; D=25μm, G=50μm)	No	Larger than 10μm
0.67 (D=50μm, G=75μm)	No	Larger than 10μm
0.8 (D=40μm, G=50μm)	No	Larger than 10μm
1 (D=50μm, G=50μm)	Yes	Smaller than 10μm
1.25 (D=50μm, G=40μm)	Yes	Smaller than 10μm
1.5 (D=75μm, G=50μm)	Yes	Smaller than 10μm
2 (D=50μm, G=25μm)	Yes	Smaller than 10μm

Similar to gap size and the post size, post gap ratio influences the particle trajectory by influencing the electric gradient. At larger ratios, the electric gradient will be larger, DEP force acting on particle will be greater, particle will thus be deflected further away from the posts. Thus using ratios greater than 1, particle will be locked in the single array (displacement mode). For ratios smaller than 1, the electric gradient will be smaller, DEP force will also become smaller, particle will easily move in zigzag mode instead of displacement mode. From the results, it is clear that the post gap ratio does affect particle trajectory. Since the ratio is connected with the electric distribution of the post area, the smaller the post gap ratio, the stronger the electric field in the post area, particle will easily move in displacement mode instead of zigzag mode. Here is the comparison between the particle trajectories using different post gap ratios.

For post gap ratio=0.5, here we show the particle trajectories in the device and how does particle move in zigzag mode:

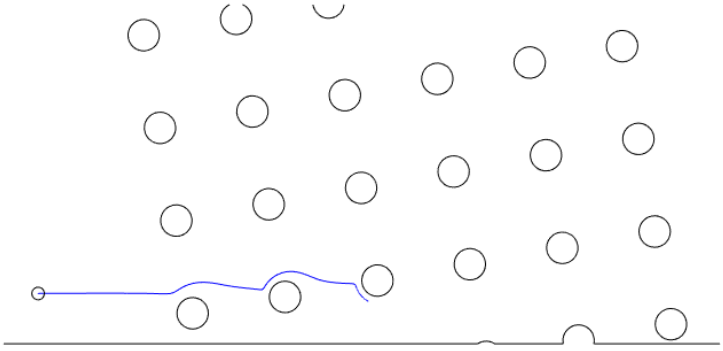

Fig 28. Migration trajectory of 10μm particle using D=25μm and G=50μm (D/G=0.5) at forcing angle α=10° in e-DLD device

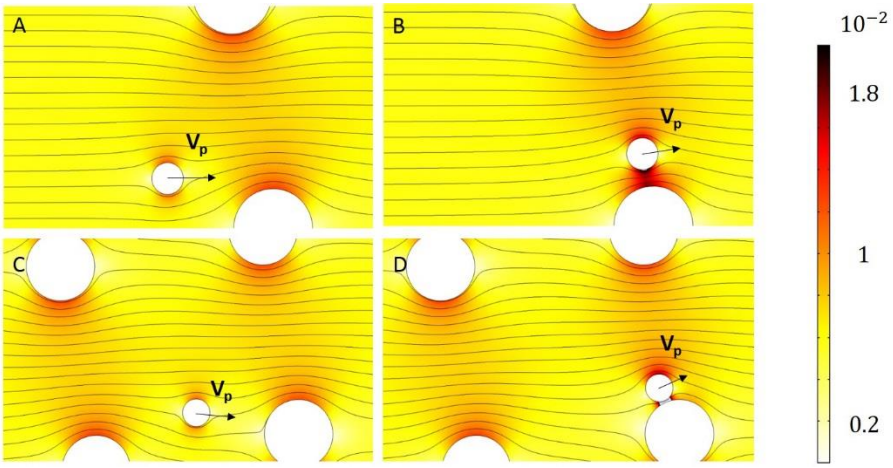

Fig 29. Migration process of 10μm particle at forcing angle α=10° using D=50μm, G=100μm (D/G=0.5), showing with non-dimensional electric field distribution and streamlines

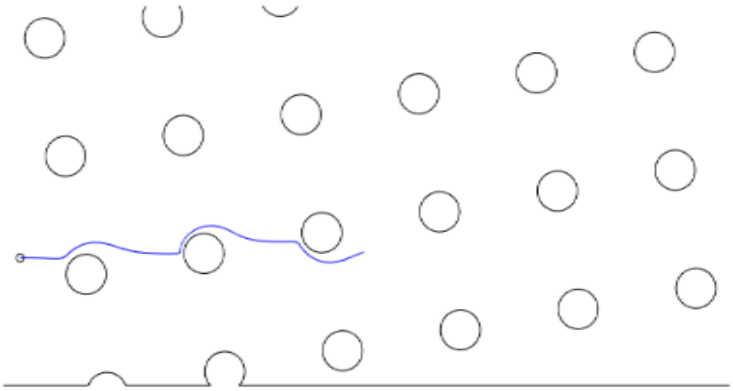

Fig 30. Migration trajectory of 10μm particle using D=50μm and G=100μm (D/G=0.5) at forcing angle α=10° in e-DLD device

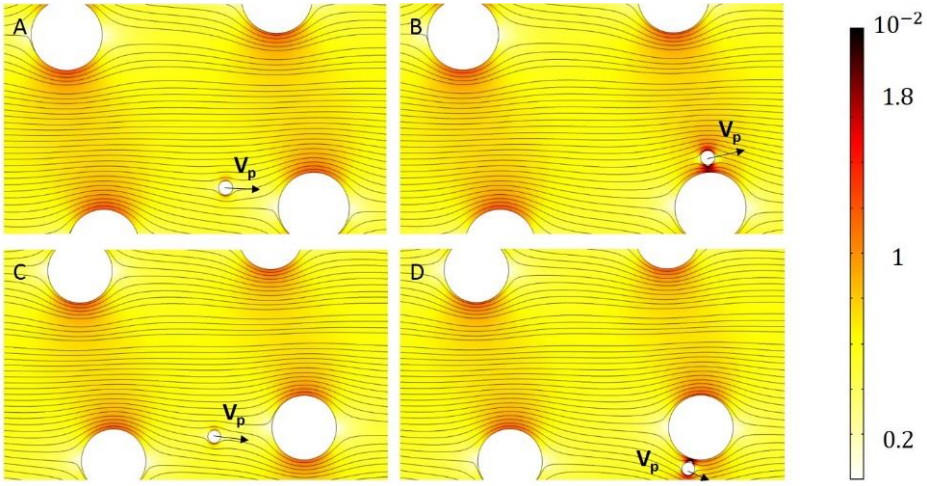

Fig 31. Migration process of 10μm particle at forcing angle α=10° using D=50μm, G=100μm (D/G=0.5), showing with electric field distribution and streamlines

For post gap ratio=1, we show the migration trajectory of both 5μm and 10μm particles:

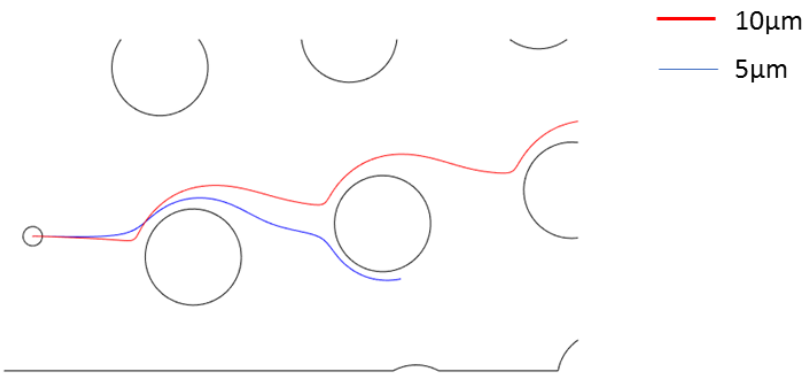

Fig 32. Migration trajectory both 5μm and 10μm particle using D=50μm and G=50μm (D/G=1) at forcing angle α=10° in e-DLD device

From the trajectories, we can see that 10μm particle move in displacement mode while 5μm particle move in zigzag mode. We can easily separate them at this situation.

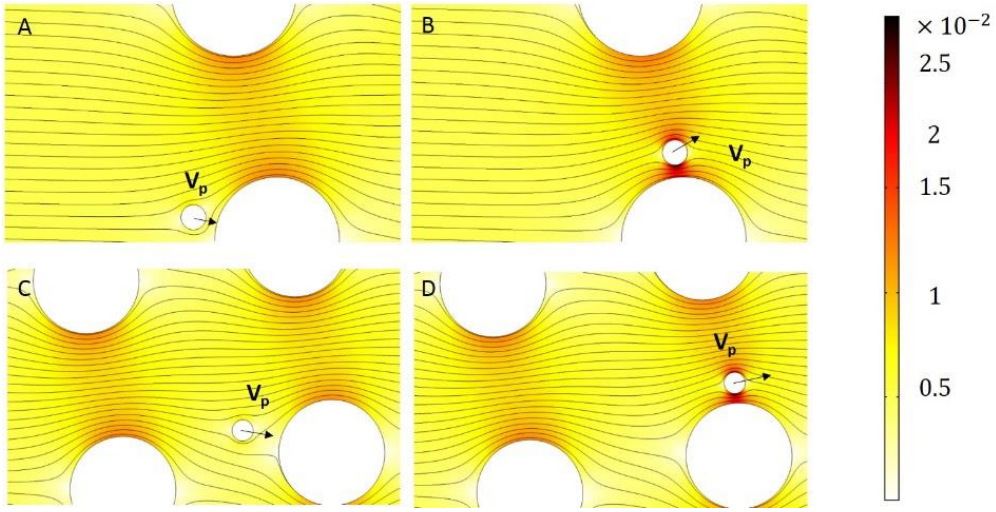

Fig 33. Migration process of 10μm particle at forcing angle α=10° using D=50μm, G=50μm (D/G=1) showing with non-dimensional electric field distribution and streamlines

For post gap ratio=2, we show the migration trajectory of both 5μm and 10μm particle:

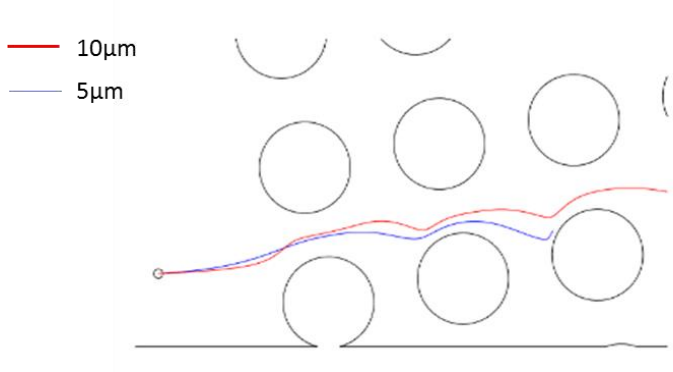

Fig 34. Migration trajectory of 5μm and 10μm particle using D=50μm and G=25μm (D/G=2) at forcing angle α=10° in e-DLD device

From the trajectories, we can see that 10μm particle move in displacement mode and 5μm particle also move in displacement mode. There is no separation happens.

From the results we show above, if we increase the post gap ratio, the electric field gradient in the post area will increase and the DEP force acting on the particle will also increase. Smaller particles will be much easier deflected from its original streamline and move in displacement mode. If we want to separate large particles from small particles, we prefer using small post gap ratio. If we want to separate two small particles, we may try using large post gap ratio so that the bigger particle may migrate in displacement mode.

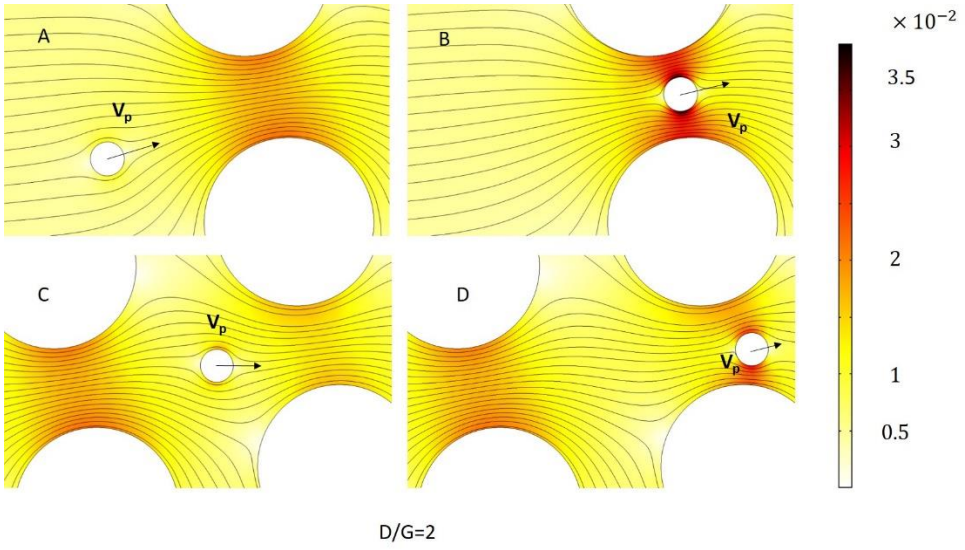

Fig 35. Migration process of 10μm particle at forcing angle α=10° using D=50μm, G=25μm (D/G=2) showing with non-dimensional electric field distribution and streamlines

For the geometry parameters, we can change either forcing angle α or post gap ratio (D/G), we can use the results we already got to find the optimum of geometry parameters to separate 5μm, 10μm and 15μm particles using forcing angle α=10° and 20° at electric field E=30KV/m.

TABLE 7. Optimization of forcing angle α and post gap ratio at E=30KV/m at forcing angle α=20°

Post gap ratio D/G / Particle size	0.5	0.67	1	1.25	2
5μm	0°	0°	0°	0°	5.4°
10μm	0°	0°	0°	19°	19.4°
15μm	0°	10°	20°	20°	20°

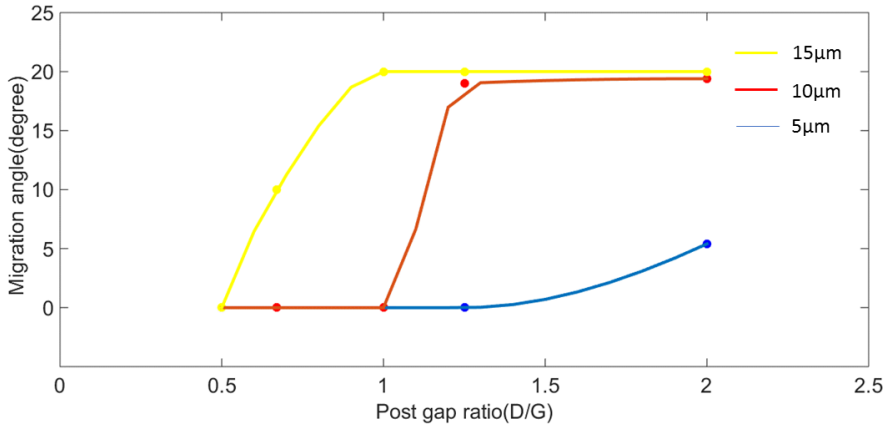

Fig 36. Migration angles of different particles using different post gap ratio (D/G)

From the above plot and table, it is evident that using forcing angle α=20°, post gap ratio D/G=1, the migration angle difference between 5μm, 10μm and 15μm particles will be the greatest. That is out optimum geometry parameters if we want to separate 5μm, 10μm and 15μm particles together. Moreover, if we want to separate two different sizes particles, using forcing angle α=20°, post gap ratio=1, we can also get the best separation efficiency of 15μm (θ=20°) and 10μm (θ=11.9°) particles. Using forcing angle α=20°, post gap ratio=0.67 or 1 we can also get the highest separation efficiency of 5μm (θ=2.9°) and 15μm (θ=17.6°) particles. Using forcing angle α=20°, post gap ratio=0.67, we can also get the best separation efficiency of 5μm (θ=0°) and 10μm (θ=19°) particles.

3.4 Electric field effect

In electrokinetic flow, the DEP force is the dominant force which should definitely influence the migration of particle, in the formula of DEP force on spherical particle:

$$\mathbf{F}_{\mathrm{DEP}} = 2\pi r^3 \varepsilon_0 \varepsilon_f f_{\mathrm{CM}} \nabla |\mathrm{E}_{\mathrm{rms}}|^2$$

In the simulation, if the particle's diameter is constant, keeping fluid property to be constant, the only factor that will influence the DEP force will be the electric gradient in the formula, since in the post area, the electric gradient is caused by the post array. Changing the electric field (same as changing potential between the channel inlet and the outlet) will change the electric gradient accordingly. Here are the results for keeping forcing angle and post gap ratio constant, the migration angle of different sizes of particles using different electric field.

TABLE 8. Migration angles of different sizes of particles using different electric field with forcing angle α=20° and post gap ratio D/G=1

Electric field (KV/m) / Particle size	10	20	30	40	50
5μm	0°	0°	0°	0°	0°
10μm	0°	0°	0°	13.1°	19.5°
15μm	4°	14.2°	20°	0°	0°

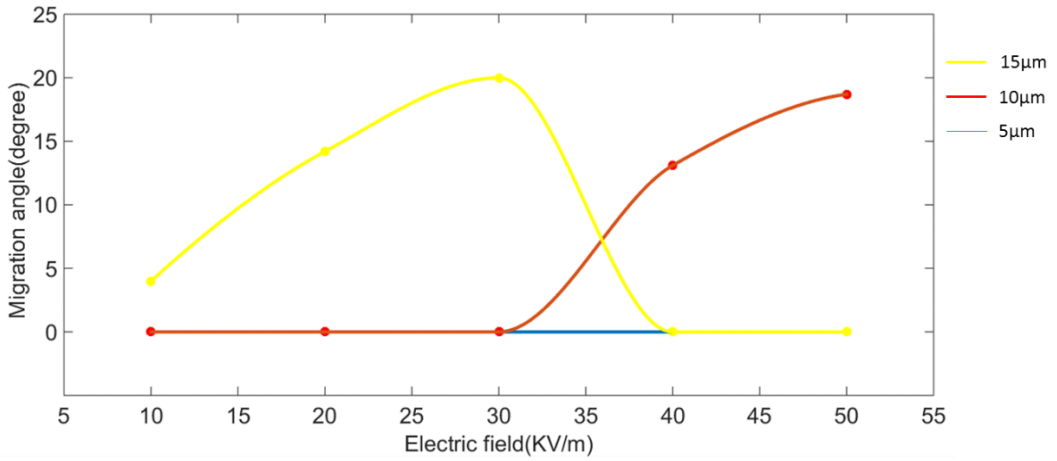

Fig 37. Migration angles for 5μm, 10μm and 15μm particles using different electric field at α=20°

Then keeping forcing angle α=20° and post gap ratio=1 fixed, using MATLAB, the diagram describing migration angle changing with electric field is obtained. It is obvious that 5μm particle always move in zigzag mode whatever the electric field is. From 10KV/m to 30KV/m, the migration angle of 10μm and 15μm particles increase with the electric field, that's because at this range, the DEP force is increasing with the growing electric field which will make the particle easier to locked to move in the [1,0] direction. After 30KV/m, when the electric field keep increasing, the DEP force the particle has will be very large so that the 15μm particles get trapped at the entrance of the post, so the migration angle can be considered as 0°. While the migration angle of 10μm particles keep increasing with the increasing electric field.

From the results we got, it is obvious that when E=30KV/m, the migration angle difference between 5μm (θ=0°), 10μm (θ=11.9°) and 15μm (θ=20°) particles will be the greatest. That is out optimum electric field if we want to separate 5μm, 10μm and 15μm particles together. What's more, if we want to separate two different sizes particles, using

forcing angle α=20°, post gap ratio=1, we can also get the best separation efficiency of 15μm (θ=20°) and 10μm (θ=11.9°) particles or 5μm (θ=0°) and 15μm (θ=20°) particles at E=30 KV/m. We can get the best separation efficiency of 5μm (θ=0°) and 10μm (θ=18.7°) particles at E= 50KV/m. This means instead of changing the post gap ratio to get the separation of 5μm and 10μm particles, we can just increase the electric field which makes the fabrication much easier.

3.5 Post shape effect

Clogging is always a problem for most mechanical filtration methods because the typical particle size is usually of the order of the gaps between obstacles. Previously, people have demonstrated that the use of an array of triangular rather than circular posts significantly enhances the performance of these devices by reducing clogging, lowering hydrostatic pressure requirements, and increasing the range of displacement characteristics in pressure driven flow[78]. DLD devices typically work well with a gap size three times that of the largest particles, thus reducing issues related to clogging. Loutherback proposed a combination of triangular posts and an oscillating flow[79] and later showed that equilateral triangular pillars with sharp vertices (rather than polygons with more vertices, rounded triangular or even circular pillars) improve the performance due to their enhanced ability to separate particles of a defined size using devices with larger gap sizes[78]. By changing the posts from the usual circular to equilateral triangular shape, an asymmetry is created in the flow profile through the gap that shifts fluid flux toward the triangle vertex.

In this simulation, every parameter is the same for circular posts and equilateral triangular posts (forcing angle α, electric field E=30KV/m, gap size=50μm), except for changing the

post shape to equilateral triangular shape which the circular post is the inscribe circle of the triangular post.

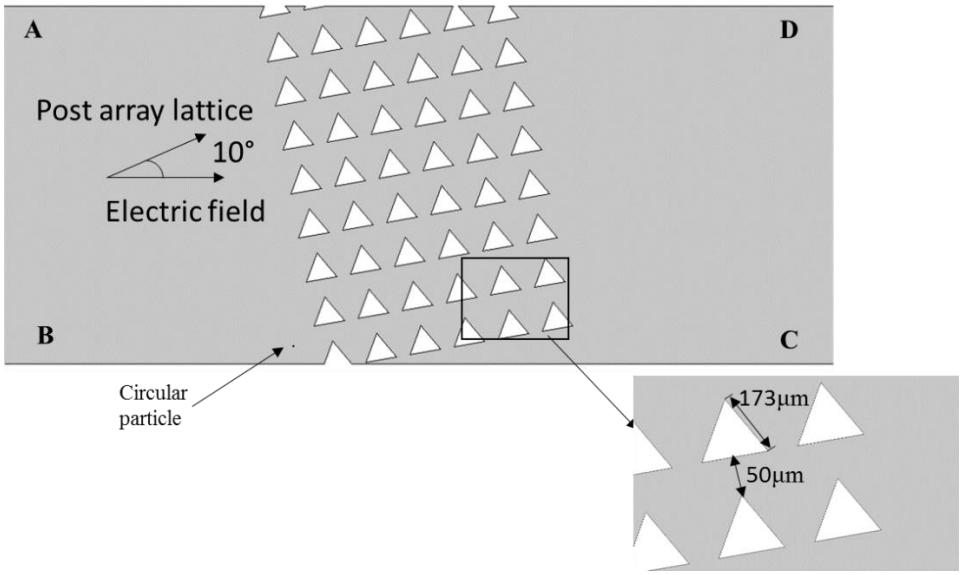

Fig 38. Computational domain using equilateral triangular posts

Interestingly, instead of following the direction of the flow field, the smaller particle is locked in the single column in post array when α=10°, and also α=15° and α=20°. Increasing the forcing angle α to 25° and 30°, the 10μm particle are still locked in the single column, the 5μm particle will follow the electric field direction, the separation phenomenon is better than the smaller post, which means when having the same gap size G and forcing angle α, the critical diameter of triangular posts will have smaller D_c than cylindrical posts. Here are the results using triangular post:

TABLE 9. Migration angles of different sizes of particle at different forcing angles using triangular post when E=30 KV/m

Forcing Angle	5°	10°	15°	20°	25°	30°
1μm	0°	0°	10.5°	9.8°	12.0°	6.6°
3μm	Locked	2.6°	6.5°	11.6°	10.9°	11°
5μm	Locked	Locked	Locked	14.0°	14.0°	18.4°
10μm	Locked	Locked	Locked	Locked	17.8°	21.5°
15μm	Locked	Locked	Locked	Locked	18.7°	22.3°
20μm	Locked	Locked	Locked	Locked	18.3°	24.3°
25μm	Locked	Locked	Locked	Locked	Locked	24.0°
30μm	Locked	Locked	Locked	Locked	Locked	Locked
Critical Diameter	1 - 3 μm	3 - 5 μm	3 - 5 μm	5 - 10 μm	20 -25 μm	25 - 30 μm

After finishing some other simulations, I found that the critical diameter when electric filed is 30KV/m is: at forcing angle 10°, the critical diameter is about 3-5μm; at forcing angle at 15°, the critical diameter is about 3-5μm; at forcing angle at 20°, the critical diameter is about 15-17μm. If we still want to separate 5μm, 10μm and 15μm particles, if it hard to find a proper forcing angle which migration angle differences of all three sizes of particles are big enough for a separation. Since at forcing angle α=5°-15°, all three sizes of particles all migrate in displacement mode. We can try to compare their migration angle at forcing angle α=20°-30°, here is the table for migration angle for three sizes of particles at forcing angle α=20°-30°.

TABLE 10. Migration angles of different sizes of particles using triangular posts at different forcing angles with E=30 KV/m

Forcing angle / Particle size	20°	25°	30°
5μm	14°	14°	18.4°
10μm	20°	17.8°	21.5°
15μm	20°	18.7°	22.3°

Not the same as using circular posts, we cannot find a proper forcing angle α to separate 5μm, 10μm and 15μm particles, so using triangular post, it is not convenient to separate 5μm, 10μm and 15μm particles together. Despite of this, using triangular post, the critical diameter of the device will be much smaller than using circular posts, which means we can separate smaller sizes of particles. We notice that at forcing angle α=10°, the migration angles of 1μm (θ=0°) and 3μm (θ=2.6°) particles are comparably small than the particles larger or equal to 5μm (θ=10°). We first show the migration trajectories of 1μm and 5μm particle using equilateral triangular posts at forcing angle α=10°. We then show the migration trajectories of 1μm and 5μm particle in the e-DLD device and discuss how the 1μm and 5μm ‘s migration angles have such big difference using the streamline in the electric field distribution.

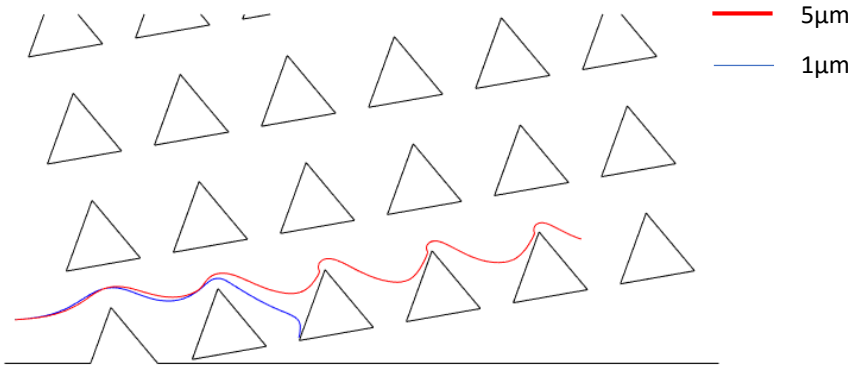

Fig 39. Separation of 1μm and 5μm particles using equilateral triangular posts at forcing angle α=10° in e-DLD device

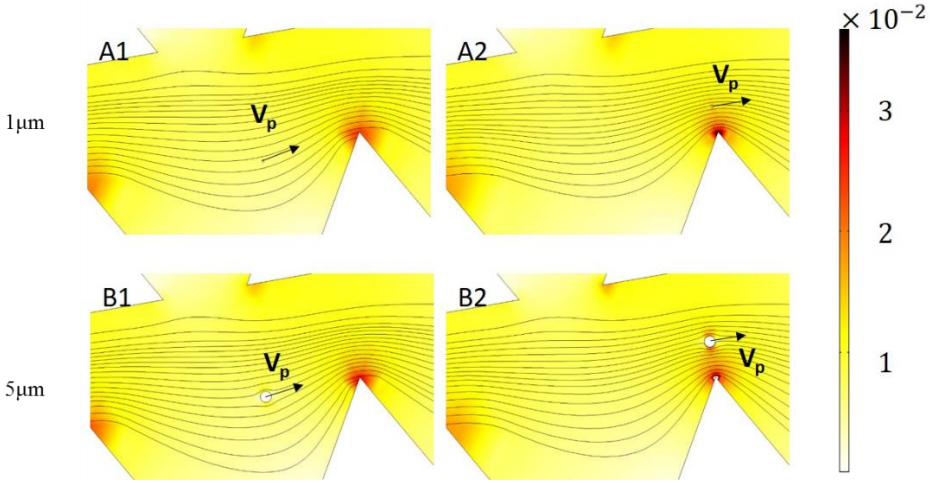

Fig 40. Migration process of 1μm and 5μm particles showing with non-dimensional electric field distribution and streamlines

During the migration, it is obvious that all the streamlines are pushed towards to the vertex of the triangular posts, where the electric field gradient is the strongest. Since 5μm particle endures much stronger electric forces (mainly DEP force), it gets deflected further away from the posts and move in the displacement mode. While electric forces

acting on 1μm particle are not large enough to deflect it far away from the posts, so 1μm particle move in zigzag mode.

Other than separating 1μm (θ=0°) and 5μm (θ=10°) at forcing angle α=10°, we also find other groups of particles we can separate using triangular posts instead of using circular posts. At forcing angle α=15°, the migration angles of 3μm (θ=6.5°) particles are comparably small than the particles larger or equal to 5μm (θ=15°); at forcing angle α=20°, the migration angles of 1μm (θ=9.8°) particles are comparably small than the particles larger or equal to 10μm (θ=20°); at forcing angle α=30°, the migration angles of both 1μm (θ=6.6°) and 3μm (θ=11°) particles are comparably small than the 5μm (θ=18.4°), 10μm (θ=21.5°) particles which is big enough for a separation.

From the simulation results, it is clear that changing the post shape from circular to triangular in a deterministic lateral displacement device results in a reduced critical particle size in electrokinetic flow. This allows smaller particles to be separated for the same gap size and forcing angle, larger forcing angle for the same critical particle size and gap, and a larger gap size for the same critical particle size and forcing angle. This last improvement is especially useful as it allows arrays to be designed with a decreased chance of clogging and lower pressure requirement for a desired flow rate. Through a series of simulations, we showed that these gains are accomplished by inducing both a more plug-like flow along the post with a sharp vertex and by producing a shift in flux toward that vertex by having a flat edge on the opposite side of the gap.

3.5 Particle shape effect

Shape-based sorting for bio-particles has recently gained traction in microfluidic devices, which are platform technologies for point-of-care medical devices, we can also use DLD device to separate particles by their shapes. Holm and Beech have performed RBC orientation based separation in a DLD device using conventional circular pillars[43,58]. They found that the RBC orientation is important for the separation. If the RBC's orientation is flat to the surface of the device, the separation critical diameter is 7μm, but if it leans to the side of the pillars, its critical separation diameter is less than 3μm. They effectively separated RBCs by creating a channel of depth 4μm to orientate the RBC flat to the surface.

For hard spherical particles, the operation of the device is straightforward, however, biological particles are often soft and non-spherical and their deformability and shape are known to influence the trajectories of the particles in DLD devices[80,81,82]. In this simulation, we want to test whether this device can be used for fractionate particles by different shapes. Keep every parameter the same and area of the circular and elliptic particle the same (since it is 2D simulation, if it is 3D simulation, the volume of the particle should be the same). For larger circular particles (10μm and 15μm), the separation may happen since the elliptic particle is not locked in single column, which may because the hydrodynamic diameter is smaller for elliptic particle; for smaller particle (5μm), there is no sign of separation. In the simulation, for most of the situations, the migration angle (θ) differences between circular and elliptic particle are very big, which are big enough for a high resolution of separation. Here are the results of

comparison between migration angle the circular particle and elliptic particle at different forcing angles when E=30 KV/m.

TABLE 11. Comparison of Circular and Elliptic particle's migration angles at different forcing angles when E=30KV/m

Particle Diameter	Particle Shape	Forcing angle α=10°	Forcing angle α=15°	Forcing angle α=20°
10 μm	Circular	10°	12.4°	0°
	Elliptic Particle(a=20μm, b=5μm)	2°	0°	0°
15 μm	Circular	10°	15°	20°
	Elliptic Particle(a=30μm, b=7.5μm)	0°	0°	1.14°

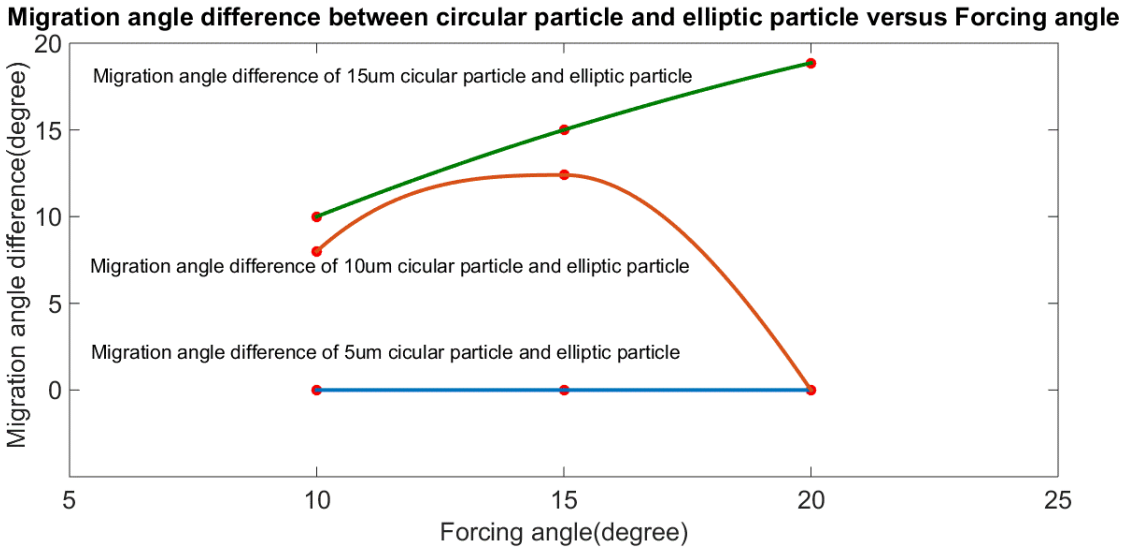

Fig 41. Migration angle differences between circular and elliptic particles

From the plot and the table, it is inferred that at forcing angle difference between the elliptic particle and circular particle reaches the maximum when using 15μm circular

particle and elliptic particle (a=30μm, b=6.5μm) at forcing angle α=20°. We will show how the 15μm circular particle and elliptic particle (a=30μm, b=6.5μm) move in the post area using the streamline in the electric field distribution.

According to the table and the plot above, it is obvious that when the particle's equivalent diameters are 10μm and 15μm for both circular and elliptic particle, the difference of the migration angle of the circular particle and the elliptic particle is big enough for a very efficient separation. For 5μm particles, both circular and elliptic particle are all in the zigzag mode which are migrating following the streamlines. For 10μm particles, the migration angle difference reaches the biggest (about 14 °) at forcing angle α=15°, for 15μm particles, the migration angle difference becomes the largest (about 17°) at forcing angle α= 20°.

We also use the different initial positions of elliptic particles. One initial position is the elliptic particle long axis parallel to the electric field, another initial position is the elliptic particle long axis perpendicular to the electric field. We find that no matter what is initial positions are, the elliptic particles always tend to migrate with its long axis parallel to the electric field in the end. That's because all the forces acting on elliptic particles make them prefer to migrate with their long axis parallel to the electric field. In this position, electric forces acting on elliptic particles will be much weaker than circular particles, and elliptic particle will thus move in zigzag mode.

We then show the migration trajectories of elliptic particle (a=30μm, b=7.5μm) and 15μm circular particle in the e-DLD device and discuss how do their migration angles have such big difference using the streamline in the non-dimensional electric field distribution.

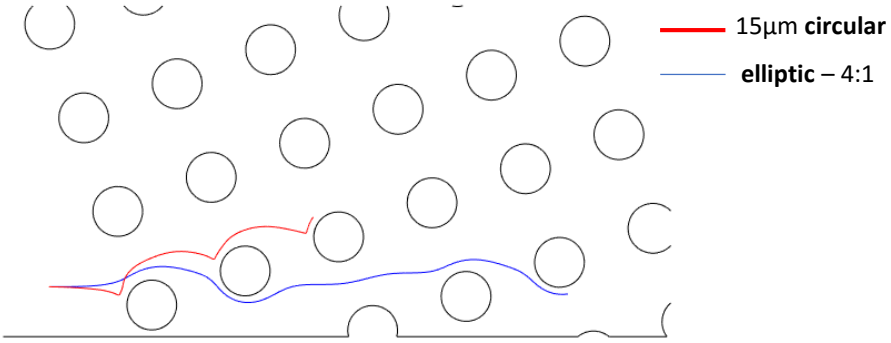

Fig 42. Separation of elliptic particle (a=30μm, b=7.5μm) and 15μm circular particles at forcing angle α=20° in e-DLD device

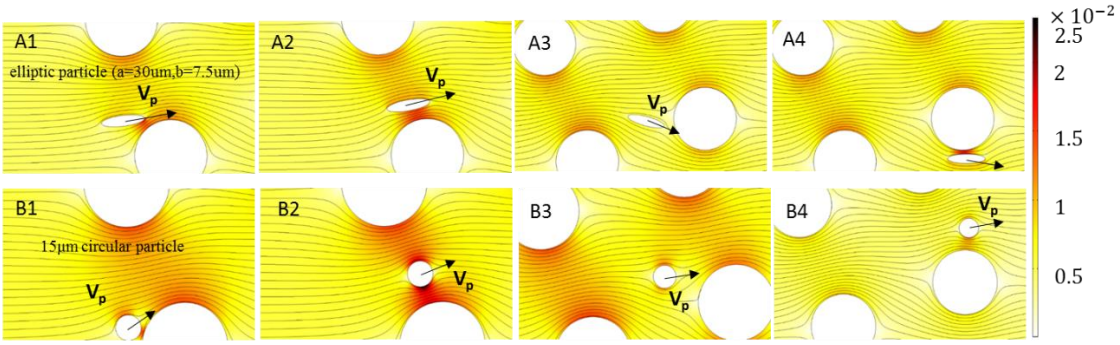

Fig 43. Migration process of elliptic particle (a=30μm, b=7.5μm) and 15μm circular particle at forcing angle α=10° showing with non-dimensional electric field distribution and streamlines

During the migration, it is evident elliptic particle is rotating all the time. The electric field gradient around the circular particle are much stronger than the elliptic particle, the

electric forces acting on the elliptic particle is very weak. The elliptic particle thus migrates in zigzag mode.

3.4 Comparison between pressure-driven DLD and e-DLD

Lots of papers of pressure-driven DLD devices have already been published, but few works have shown that e-DLD devices have lots of advantages over pressure-driven DLD. Here we use both 10μm particle and forcing angle α=10° in a pressure-driven DLD device and a e-DLD device (E=30KV/m) at almost the same entrance fluid velocity. As we showed in the previous section, in e-DLD device, at forcing angle α=10°, 10μm particle move in the displacement mode. In pressure-driven DLD device, the 10μm particle move in zigzag mode.

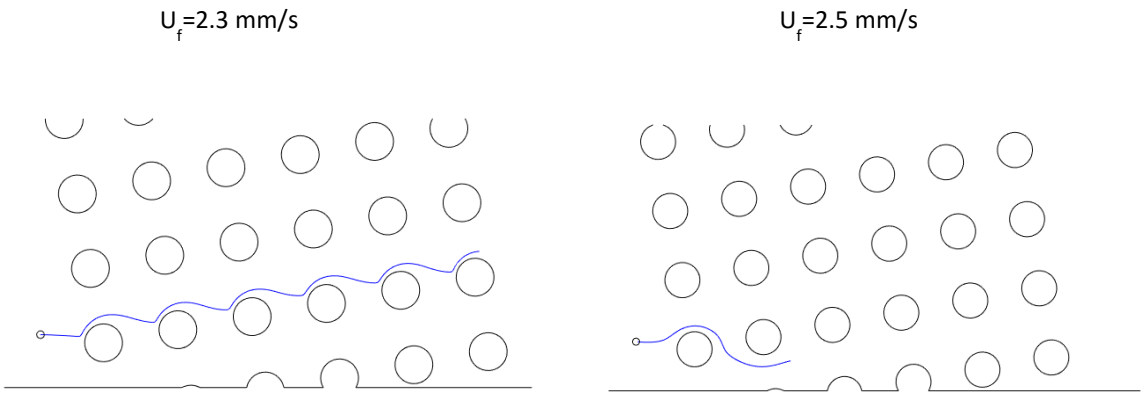

Fig 44. 10μm particle trajectories using e-DLD device (left) and pressure driven DLD device (right) at forcing angle α=10°

The reason why the 10μm particle in different devices migrate at different mode is the forces acting on particles in these two devices are quite different. In e-DLD device, particle will mainly endure DEP force and other electric forces, when particles move close to the post, the electric forces acting on the particles are quite large, especially at

vertical direction. The large vertical component of electric forces acting on the particles deflect them very far away from the posts, thus, the particles migrate in displacement mode. While in pressure-driven DLD device, the hydrodynamic forces acting on the particles are too small, so that the particle won't be deflected far enough from the posts. Particles will follow the streamline and migrate in zigzag mode. Actually, at forcing angle α=10°, even we use 30μm particle, it still migrates in zigzag mode which is very inconvenient if we want to separate this size range (10μm-30μm) of particles. If we want to separate this size range of particles, we can decrease the forcing angle to about α=5°, which means we need a much longer channel to separate particles. Or we can decrease the gap size, which may cause the particle clogging and will increase the difficulty of manufacture.

From the results we get, there are some advantages of e-DLD over pressure driven DLD. Using the same geometry, e-DLD can separate smaller particles. Also, if we want to separate certain particles sizes using both pressure-driven DLD and e-DLD devices, we can have larger gap size or larger forcing angle in e-DLD device. These means we can use larger gap size which makes the manufacture much easier or we can use rather short channel to separate similar sizes of particles to save resources. In addition to extending the versatility of DLD with an alternative driving field, the use of electric fields opens the possibility to on-line control of the orientation of the driving field depending on the sample.

3.5 Limitations

We have numerically got the separation of particles based on size using both circular and equilateral triangular posts in e-DLD devices using ALE methods. We also showed the separation of particles in different shapes. However, in ALE methods, the trajectories of particles we got is the combination of different cases in which we can only simulate one particle at a time. In experiment and real applications in medical and biological field, people try to separate lots of particles together. There are few things we should consider. Firstly, in our simulation, particles' initial positions are all at the bottom of the post array. In the experiment, there will be two inlets for both buffer solution and the particle solution. Buffer solution will come at the top inlet while the particle solution will come at the bottom inlet. In order to concentrate the particle at the bottom of the post array, we can control the entrance flow rate of both buffer solution and the particle solution at certain ratio.

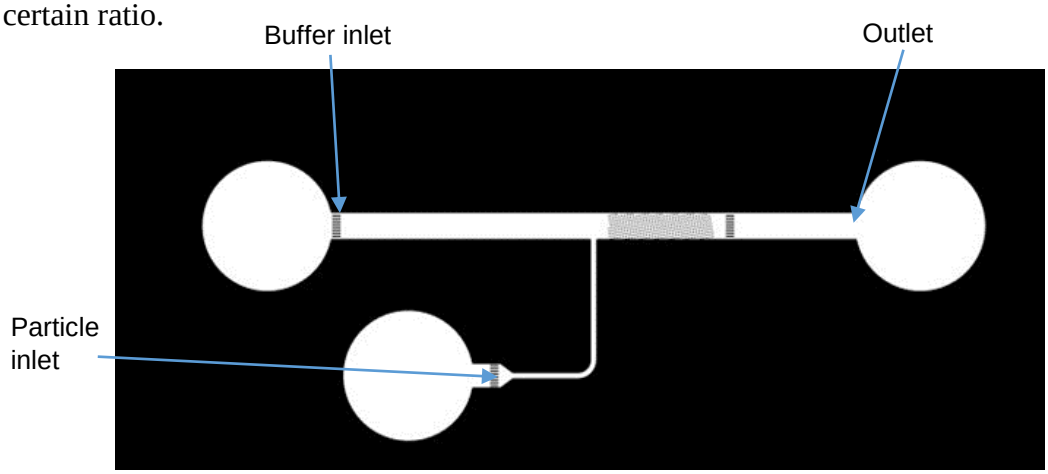

Fig 44. Schematics of microchannel used in experiment

Second of all, we should also consider the particle to particle interaction. Since in experiment, there will be thousands of particle in the microchannel, when two particles

get close to each other, the local electric field around them will be changed. Since it is negative DEP, two particles will push each other away from their original streamlines. This will definitely influence the particles' trajectories and the particle movement will be more chaotic. Particles supposed to move in displacement mode may migrate in zigzag mode and particles supposed to move in zigzag mode may migrate in displacement mode. The separation phenomena will be weakened because of the particle to particle interaction. What we can do is to try to use less concentrated particle solution and thus to decrease the effect of the particle to particle interaction. It is better to find an optimum particle solution concentration which we can both have reasonable separation phenomena and high throughput.

CHAPTER FOUR

CONCLUSIONS AND FUTURE WORK

4.1 Conclusions

We have numerically demonstrated the simplicity and potential of using an e-DLD device to achieve particle separation. This e-DLD device can easily to change the relative orientation of the driving field with respect to the array of posts.

First of all, we have proved numerically a continuous, two-dimensional separation of 5μm, 10μm and 15μm-diameter rigid circular particles in an e-DLD device. We have shown that, the observed deterministic kinetics of the particles motion including directional locking, and our understanding of those systems can be applied to describe and analyze the behavior in the e-DLD devices. We have performed a comprehensive set of simulations that using different orientations of the driving electric field, and showed the potential for separation at specific forcing angles. We have also discussed that the first transition angle exhibits a large dependence on particle size, with a difference of nearly 15° between the smallest and largest particles, which suggests the use of relatively small forcing angles to optimize the resolution of the system. We have also observed sharp transitions between locking directions, indicating the potential for high size resolution of the e-DLD device.

Then we have discussed several factors that affect the separation of the particles in e-DLD device, such as electric field, forcing angle, post gap ratio, post shape and particle

shape. We use the migration angle difference of different particles as the criteria for separation efficiency.

We have explored certain orientations of the driving field with respect to the array of obstacles and showed that, at specific forcing-angles, particles of different sizes migrate in different directions, thus enabling continuous, two-dimensional separation in electrokinetic flow. We have also showed the reason why certain size of particle will transit from displacement mode to zigzag mode with increasing forcing angle. We have also found the optimum forcing angle to separate three different sizes of particles or two different sizes of particles.

We have also discussed the effect of the post gap ratio on particle separation, the larger the ratio is, the easier particle would migrate in displacement mode. We have showed that forcing angle α=20° and post gap ratio D/G=1 is the optimum geometry parameters if we want to separate 5μm, 10μm from 15μm-diameter rigid circular particles. The optimum parameters to separate 5μm, 10μm from 15μm-diameter rigid circular particles are forcing angle α=20°, post gap ratio D/G=1 and electric field E=30 KV/m. The optimum parameters to separate 5μm from 10μm-diameter rigid circular particles are forcing angle α=20°, post gap ratio D/G=1 and electric field E=50 KV/m.

The post shape also plays an important role on separation. We used equilateral triangular under the same conditions with circular posts. We have noticed that at forcing angle α=10°, we can easily separate 1μm and 5μm particle. This allows smaller particles to be separated in e-DLD devices. Compared to e-DLD device using circular posts, we can use the same gap size and forcing angle, larger forcing angle for the same critical particle size

and gap, and a larger gap size for the same critical particle size and forcing angle using equilateral triangular posts.

We then looked into the particle shape effect using elliptic particles. It was found that an elliptic particle behaves like a smaller sized circular particle due to its preferred orientation in electric field. In this way, we have been able to separate circular particle and elliptic particle easily with equal area in high resolution.

In the end, we have compared the traditional pressure-driven DLD device with e-DLD device. With the same geometry, e-DLD device is capable of separating much smaller particles. Alternatively, pressure driven-DLD requires a smaller gap size and/or a smaller forcing angle to implement the same particle separation as the traditional DLD does. This means pressure-driven DLD devices is harder to manufacture and using e-DLD device will considerably ease the DLD device fabrication and shorten the length of the post array.

4.2 Future work

We have showed some factors that influence the separation of e-DLD device, but there are still other properties we can study. We also need to verify the simulation results by experiments.

First of all, we can look into the particle charge effect. As we mentioned in previous chapter, the particle's net velocity in a straight channel is the addition for electrokinetic velocity and DEP velocity. The electrokinetic velocity is determined by the difference between the zeta potential of the channel wall and the particle. The electrokinetic velocity

(U_{EK}) is the main transition velocity for particle to immigrate in the channel. Keep wall zeta potential the same, if we use particle with different zeta potential (other properties are the same), which the electrokinetic velocity will be different. If the difference between the zeta potential of the particle and the wall increase, the electrokinetic velocity will increase, which will in turn cause the particle immigrate faster in the channel. By using different particle zeta potential, we can also separate particle by their charge. Secondly, all the simulations we did were based on rigid particles, but in real application in medical or clinic engineering, most of the cells are deformable (RBC, WBC), which won't apply for our previous simulations. It is very important to find a way to separate by their deformability.

In the end, it is also very important to do some experiments to verify our simulation results. Since in experiments, some factors we did not consider in the simulation may also have an impact on the results we get.

CHAPTER FIVE

REFERENCES

1 Whitesides, G. M., *Nature*. 2006, 442, 368-373.

2 McGrath, J., Jimenez, M., Bridle, H., *Lab Chip*. 2014 Nov 7; 14(21):4139-58.

3 Bhagat, A. A. S., Bow, H., Hou, H. W., Tan, S. J., Han, J. and Lim, C. T., *Med. Biol. Eng. Comput.* 2010, 48, 999–1014.

4 Jackson, E. L. and H. Lu, *Curr. Opin. Chem. Eng*. 2013, 2, 398–404.

5 Kersaudy-Kerhoas, M., Dhariwal, R. and Desmulliez, M., *IET Nanobiotechnol.* 2008, 2, 1-13.

6 Yamada, M., Nakashima, M. and Seki, M., *Anal. Chem.* 2004, 76, 5465.

7 Takagi, J., Yamada, M., Yasuda, M. and Seki, M., *Lab Chip*. 2005, 5, 778.

8 Yamada, M. and Seki, M., *Anal. Chem.* 2006, 78, 1357.

9 Choi, S. and Park, J.-K., *Lab Chip*. 2007, 7, 890.

10 Chou, C.-F., Bakajin, O., Turner, S. W. P., Duke, T. A. J., Chan, S. S., Cox, E. C., Craighead, H. G. and Austin, R. H., *Proc. Natl. Acad. Sci. U. S. A.* 1999, 96, 13762.

11 Zhang, X. L., Cooper, J. M., Monaghan, P. B. and Haswell, S. J., *Lab Chip*. 2006, 6, 561.

12 Autebert, J., Coudert, B., Bidard, F.-C., Pierga, J.-Y., Descroix, S., Malaquin, L. and Viovy, J.-L., *Methods*. 2012, 57(3). 297–307.

13 Devasenathipathyl, S., Santiago, J. G., Yamamoto, T., Sato, Y., Hishida, K., *7th lnternat~onal Conference on Miniaturized Chemical and Blochemlcal Analysts Systems, October 5-9, 2003*.

14 DuBose, J., Zhu, J., Patel, S., Lu, X., Tupper, N., Stonaker, J. M. and Xuan, X., *J. Micromech. Microeng*. 24 (2014) 115018 (7pp).

15 Zhu, J., Canter, R. C., Keten, J., Vedantam, P., Tzeng, T. J., Xuan, X., *Microfluid Nanofluid*. (2011) 11:743–752.

16 Collins, D. J., Alan, T. and Neild, A., *Lab Chip*. 2014, 14, 1595–1603.

17 Beech, J. P., Jonsson, P. and Tegenfeldt, J. O., *Lab Chip*. 2009,9, 2698–2706

18 Chang, S. and Cho, Y.-H., A continuous multi-size particle separator using negative dielectrophoretic virtual pillars induced by a planar spot electrode array. 2007.

19 Devendra, R. and Drazer, G., *Anal. Chem.* 2012, 84, 10621–10627.

20 Beech, J. P., Tegenfeldt, J. O., Conference Paper, 2009.

21 Jiang, M., Budzan, K., Drazer, G., *Microfluidics and Nanofluidics*, 2015, Volume 19, issue 2, pp 427-434

22 Frechette, J. and Grazer, G., *J. Fluid Mech.* (2009), vol. 627, pp. 379–401.

23 Ranjan, S., Zeming, K.K., Jureen, R., Fisher, D., Zhang, Y., *Lab Chip.* 2014 Nov 7;14(21):4250-62

24 Inglis, D. W., *Applied Physics Letters* 94, 013510 (2009)

25 Holm, S. H., Beech, J. P., Barrett, M. P., Tegenfeldt, J. O., *Lab Chip*. 2011 Apr 7;11(7):1326.

26 Hanasoge, S., Devendra, R., Diez, F. J., Drazer, G., *Microfluid Nanofluid*. 2015.

27 Helmholtz, H. V., Studien uber elctrische grenschichten, *Ann. der Physik und Chimie,* 1879,**7**, 337–387.

28 Smoluchowski, M. von, Contribution a la theorie de l'endosmose electrique et dequelquesphenomenes correlatifs, Bull. *International de l'Academie des Sciences de Cracovie,* 1903, 8,182–200.

29 Dukhin, S. S., Derjaguin, B. V., *Electrokinetic Phenomena, in Surface and Colloid Science*, vol. 7, E. Matijevic (Ed.),Wiley, 1974.

30 H. Bruus, *Theoretical microfluidics*, 2nd ed., MIC – Department of Micro and Nanotechnology, Technical University of Denmark, 2005.

31 Ai, Y., Qian, S., *Electrokinetic Particle Transport In Micro-/Nanofluidics.* 2012.

32 Kang, Y. J., Cetin, B., Wu, Z. M., Li, D. Q., *Electrochimica Acta.* 54 (2009) 1715–1720.

33 K. H. Bhatt, S. Grego, O. D. Velev, An AC electrokinetic technique for collection and concentration of particles and cells on patterned electrodes, *Langmuir* 21 (2005) 6603–6612.

34 N. Demierre, T. Braschler, P. Linderholm, U. Seger, H. van Lintel, P. Renaud, Characterization and optimization of liquid electrodes for lateral dielectrophoresis, *Lab Chip* 7 (2007) 355–365.

35 T-S Leu, H-Y Chen, F-B Hsiao, Studies of particle holding, separating, and focusing using convergent electrodes in microsorters, *Microfluid Nanofluid* 1 (2005) 328–335.

36 S. K. Srivastava, A. Gencoglu, A. R. Minerick, DC insulator dielectrophoretic applications in microdevice technology: a review, *Anal. Bioanal. Chem*. 399 (2010) 301–321.

37 B. Cetin, D. Li, Dielectrophoresis in microfluidics technology, *Electrophoresis* 32 (2011) 2410–2427.

38 B. H. Lapizco-Encinas, B. A. Simmons, E. B. Cummings, Y. Fintschenko, Insulator-based dielectrophoresis for the selective concentration and separation of live bacteria in water, *Electrophoresis* 25 (2004) 1695-1704.

39 L. M. Barrett, A. J. Skulan, A. K. Singh, E. B. Cummings, G. J. Fiechtner, Dielectrophoretic Manipulation of Particles and Cells Using Insulating Ridges in Faceted Prism Microchannels, *Anal. Chem.* 77 (2005) 6798–6804.

40 K. H. Kang, Y. Kang, X. Xuan, D. Li, Continuous separation of microparticles by size with direct current-dielectrophoresis, *Electrophoresis* 27 (2006) 694–702.

41 Saucedo-Espinosa, M. A., LaLonde, A., Gencoglu, A., Romero-Creel, M. F., Dolas J. R., Lapizco-Encinas, B. H., *Electrophoresis.* 2016 Jan; 37(2):282-90.

42 Huang, L. R., Cox, E. C., Austin, R. H. and Sturm, J. C., *Science*. 2004, 304, 987–990.

43 Balvin, M., Sohn, E., Iracki, T., Drazer, G. and Frechette, J., Phys. *Rev. Lett.* 2009, 103, 078301.

44 Inglis, D. W., Davis, J. A., Austin, R. H. and Sturm, J. C., *Lab Chip*. 2006, 6, 655–658.

45 Beech, J. P., Jonsson, P. and Tegenfeldt, J. O., Lab Chip, 2009,9, 2698–2706

46 Beech, J. P., Deterministic Lateral Displacement Devices, MSc, Lund University, 2005

47 Zheng, S., Yung, R., Tai, Y.-C. and Kasdan, H., Deterministic lateral displacement MEMS device for continuous blood cell separation. 2005.

48 Davis, J. A., Inglis, D. W., Morton, K. J., Lawrence, D. A., Huang, L. R., Chou, S. Y., Sturm, J. C. and Austin, R. H., *Proc. Natl. Acad. Sci. U. S. A.* 2006, 103,14779–14784.

49 Holm, S. H., Beech, J. P., Barrett, M. P., and Tegenfeldt, J. O., *Lab Chip*. 2011, 11, 1326–1332.

50 Loutherback, K., D'Silva, J., Liu, L., Wu, A., Austin, R. H. and Sturm, J. C., *AIP Adv.* 2012, 2, 042107.

51 Gleghorn, J. P., Pratt, E. D., Denning, D., Liu, H., Bander, N. H., Tagawa, S. T., Nanus, D. M., Giannakakou, P.A. and Kirby, B. J., Capture of circulating tμmor cells from whole blood of prostate cancer patients using geometrically enhanced differential immunocapture (GEDI) and a prostate-specific antibody. 2010.

52 Kirby, B. J., Jodari, M., Loftus, M. S., Gakhar, G., Pratt, E. D., Chanel-Vos, C., Gleghorn, J. P., Santana, S. M., Liu, H., Smith, J. P., Navarro, V. N., Tagawa, S. T., Bander, N. H., Nanus, D. M., Giannakakou, P., Functional Characterization of Circulating Tumor Cell with a Prostate-Cancer-Specific Microfluidic Device. 2012.

53 Inglis, D. W., Morton, K. J., Davis, J. A., Zieziulewicz, T. J., Lawrence, D. A., Austin, R. H. and Sturm, J. C., *Lab Chip*. 2008, 8, 925–931.

54 Lapizco-Encinas, B. H., Simmons, B. A., Cummings, E. B., Fintschenko, Y., *Electrophoresis.* 471 2004, 25, 1695-1704.

55 Moncada-Hernández, H., Lapizco-Encinas, B. H., *Anal. Bioanal. Chem.* 2010, 396, 1805-1816.

56 Pysher, M. D., Hayes, M. A., *Anal. Chem.* 2007, *79*, 4552-4557.

57 Kang, Y., Li, D., Kalams, S., Eid, J., *Biomed. Microdev.* 2008, *10*, 243-249.

58 Abdallah, B. G., Chao, T.-C., Kupitz, C., Fromme, P., Ros, A., *ACS Nano.* 2013, *7*, 9129-9137.

59 Nakano, A., Camacho-Alanis, F., Chao, T.-C., Ros, A., *Biomicrofluidics.* 2012, *6*, 034108-*478* 034113.

60 Nakano, A., Chao, T. C., Camacho-Alanis, F., Ros, A., *Electrophoresis.* 2011, *32*, 2314-2322.

61 Gallo-Villanueva, R. C., Rodríguez-López, C. E., Díaz-de-la-Garza, R. I., Reyes-Betanzo, C., Lapizco-Encinas, B. H., *Electrophoresis.* 2009, *30*, 4195-4205.

62 Camacho-Alanis, F., Gan, L., Ros, A., *Sens. Actuator B-Chem.* 2012, *173*, 668-675.

63 Luo, J., Abdallah, B. G., Wolken, G. G., Arriaga, E. A., Ros, A., *Biomicrofluidics.* 2014, *8*, 021801.

64 Lapizco-Encinas, B. H., Davalos, R., Simmons, B. A., Cummings, E. B., Fintschenko, Y., *J. 486 Microbiol. Methods.* 2005, *62*, 317-326.

65 Masuda, T., Maruyama, H., Honda, A., Arai, F., *PLoS ONE.* 2014, *9*, e94083.

66 Gencoglu, A., Olney, D., LaLonde, A., Koppula, K. S., Lapizco-Encinas, B. H., *Electrophoresis.* 2014, *35*, 363-373.

67 Zellner, P. A., Sahari, A., Hosseini, Y., Behkam, B., Agah, M., in *Annual International Conference of the IEEE Engineering in Medicine and Biology Society.* 2012, 2012, 6285-6288.

68 Saucedo-Espinosa, M. A., LaLonde, A., Gencoglu, A., Romero-Creel, M. F., Dolas, J. R., Lapizco-Encinas, B. H., *Electrophoresis* 2016, 37, 282-290

69 Xuan, X. C. and Li, D. Q., *J. Micromech. Microeng*. 2006,16, 62.

70 Du, S., Drazer, G., *J. Micromech. Microeng*. 25 (2015) 114002 (8pp).

71 Ai, Y., Joo, S. W., Jiang, Y., Xuan, X., Qian, S., *Biomicrofluidics.* 2009, *3*, 022404.

72 Ai, Y., Beskok, A., Gauthier, D. T., Joo, S. W., Qian, S., *Biomicrofluidics.* 2009, *3*, 044110.

73 Ai, Y., Joo, S. W., Jiang, Y., Xuan, X., Qian, S., *Electrophoresis.* 2009, *30*, 2499–2506.

74 Ai, Y., Park, S., Zhu, J., Xuan, X., Beskok, A., Qian, S., *Langmuir.* 2010, *26*, 2937–2944.

75 Ai, Y., Qian, S., *J. Colloid Interface Sci.* 2010, *346*, 448–454.

76 Ai, Y., Qian, S., Liu, S., Joo, S. W., *Biomicrofluidics.* 2010,*4*, 013201.

77 Ai, Y., Mauroy, B., Sharma. A., Qian, S., *Electrophoresis.* 2011, *32*, 2282–2291.

78 Loutherback, K., Chou, K. S., Newman, J., Puchalla, J., Austin, R. H., Sturm, J. C., *Microfluid Nanofluid*. (2010) 9:1143-1149.

79 Loutherback, K., Newman, J., Puchalla, J., Austin, R.H., Sturm, J.C., *Phys. Rev. Lett.* 102, 045301 (2009).

80 Beech, J. P., Holm, S. H., Adolfsson, K. and Tegenfeldt, J. O., *Lab Chip*, 2012, 12, 1048–1051.

81 Inglis, D. W., PhD thesis: Microfluidic Devices for Cell Separation, Princeton University, 2007.

82 Davis, J. A., PhD Thesis: Microfluidic Separation of Blood Components through Deterministic Lateral Displacement, Princeton University, 2008.